# The Rise of Magma Through the Crust

# 3

## 3.1 Introduction

After the fundamentals summarized in Chaps. 1 and 2, this chapter introduces the second and main part of the book. This part, from this Chapter to Chap. 9, focuses on the general path followed by magma in passing through the crust, ideally consisting of its rise, shallow accumulation, shallow transfer and eruption. In particular, the path begins with the rise of magma through the crust (described in this chapter). The rise of magma is a requisite for promoting shallow magma accumulation, and thus developing magma chambers (Chap. 4). A significant withdrawal of magma from a chamber may determine a vertical collapse, or caldera, at the surface (Chap. 5). A withdrawal of magma rising towards the surface may promote the instability of the flank of a volcanic edifice, triggering lateral, or sector, collapse (Chap. 6). In both types of collapse, the modifications in the shape of the volcanic edifice introduce deviations from the expected patterns of shallow transfer of magma feeding eruptions (Chap. 7). Both the shallow accumulation and transfer of magma can be detected and tracked through a multi-parametric volcano monitoring system (Chap. 8), which allows understanding the state of an active volcano, ultimately providing the basis for eruption forecasting (Chap. 9).

In more detail, this chapter considers the general processes controlling the rise of magma within the crust, progressing from classic studies on magma rise through diapirs to modern perspectives, which challenge or anyway limit diapiric ascent in favour of dike propagation. As regards dikes, this chapter considers the general mechanisms of dike propagation and arrest, independently of the level of nucleation of the dikes, may this be in the lower or upper crust. The description of the more specific conditions controlling dike nucleation from magma chambers and dike propagation approaching the surface and within volcanic edifices are considered in Chaps. 4 and 7, respectively.

The main aims of this chapter are thus to define the:

- mechanisms of development of magmatic diapirs;
- mechanisms of propagation and arrest of dikes;
- general conditions determining the rise of magma through diapirs or dikes in the crust.


V. Acocella, *Volcano-Tectonic Processes*, Advances in Volcanology,
https://doi.org/10.1007/978-3-030-65968-4_3

## 3.2 Magmatic Diapirs

The rise of magma through the crust has been ascribed for decades to the development of diapirs. A **diapir** is a massive magmatic intrusion piercing through the surrounding country rock mainly through density contrast, or buoyancy, between the lighter magma and the denser crust. As felsic magma is lighter and more buoyant, diapirs commonly have a felsic, preferably granitoid, composition. Diapirs, consisting of massive and relatively viscous magma, commonly interrupt their ascent and emplace at depth, where they slowly crystallize and form intrusions. The emplacement of diapirs has been also often invoked to explain the formation of **plutons**, which are massive and solidified intrusions of magma accumulated in the crust (see Chap. 4). A rising magmatic diapir is expected to have an inverted teardrop shape, with domed roof, evolving towards a mushroom-like shape during its final emplacement, that is when the intrusion starts spreading laterally (Fig. 3.1).

The rise of a diapir occurs through the viscous flow of the massive magma body coupled with that of the surrounding host rock. In this context, a rising diapir is accompanied by marked lateral gradients within the country rock, with the temperature and viscosity rapidly decreasing and increasing away from the intrusion contacts, respectively. Conversely, ascent velocity is largest (and positive) at the intrusion centre, to become negative (highlighting downward flow) within a thermally softened zone of the country rock next to the intrusion. The time scale of granitoid diapirism over crustal distances is estimated on the order of $10^4$–$10^5$ years (Mahon et al. 1988).

Several studies have analysed the generation and development of diapirs in theory and experiments. These are consistent in describing an overall variation in the shape of the ascending diapir from its mobilization to its arrest, identifying three main stages: initiation, rise and emplacement (Fig. 3.2; Berner et al. 1972; Dixon 1975; Ramberg 1981; Bittner and Schmeling 1995). These are described in the sections below.

### 3.2.1 Diapir Initiation

Diapirs initiate as **Rayleigh–Taylor instabilities**, that are instabilities which develop along the interface between immiscible fluids, with a lighter fluid below a heavier one. In the case of magmatic diapirs, the lighter magma flows and rises within the denser country rock of the viscous lower crust (e.g., Turcotte and Schubert 1982, and references therein). The interface between the magma and the country rock is in a state of unstable equilibrium, as any perturbation or disturbance is amplified by the Earth's gravity, with the result that the heavier fluid tends to be displaced downward and an equal volume of lighter fluid upward. These disturbances grow, so that an increasing amount of denser material is displaced downward and lighter material upwards, leading to an overall decrease in potential energy of the system.

The size and rate of growth of an instability depend upon several boundary conditions, including the density and viscosity contrasts between the two fluids, the thickness of the upper layer and, in the case of magma, its degree of partial melting (Biot and Odè 1965). Theoretical calculations suggest that the wavelength associated with a dominant disturbance is $\sim 2.56\ T_u$, where $T_u$ is the thickness of the upper layer, indicating that the thinner is the upper layer the more closely spaced are the instabilities. This theoretical relationship is in agreement with the distribution of salt diapirs in nature (Jackson and Talbot 1986). The wavelength of the disturbance also depends upon the viscosity contrast: as the viscosity of the upper layer increases, the dominant wavelength increases and its rate of amplification (i.e., vertical growth of wavelength) decreases. Assuming any viscosity contrast null, the time of growth of the dominant disturbance is given by:

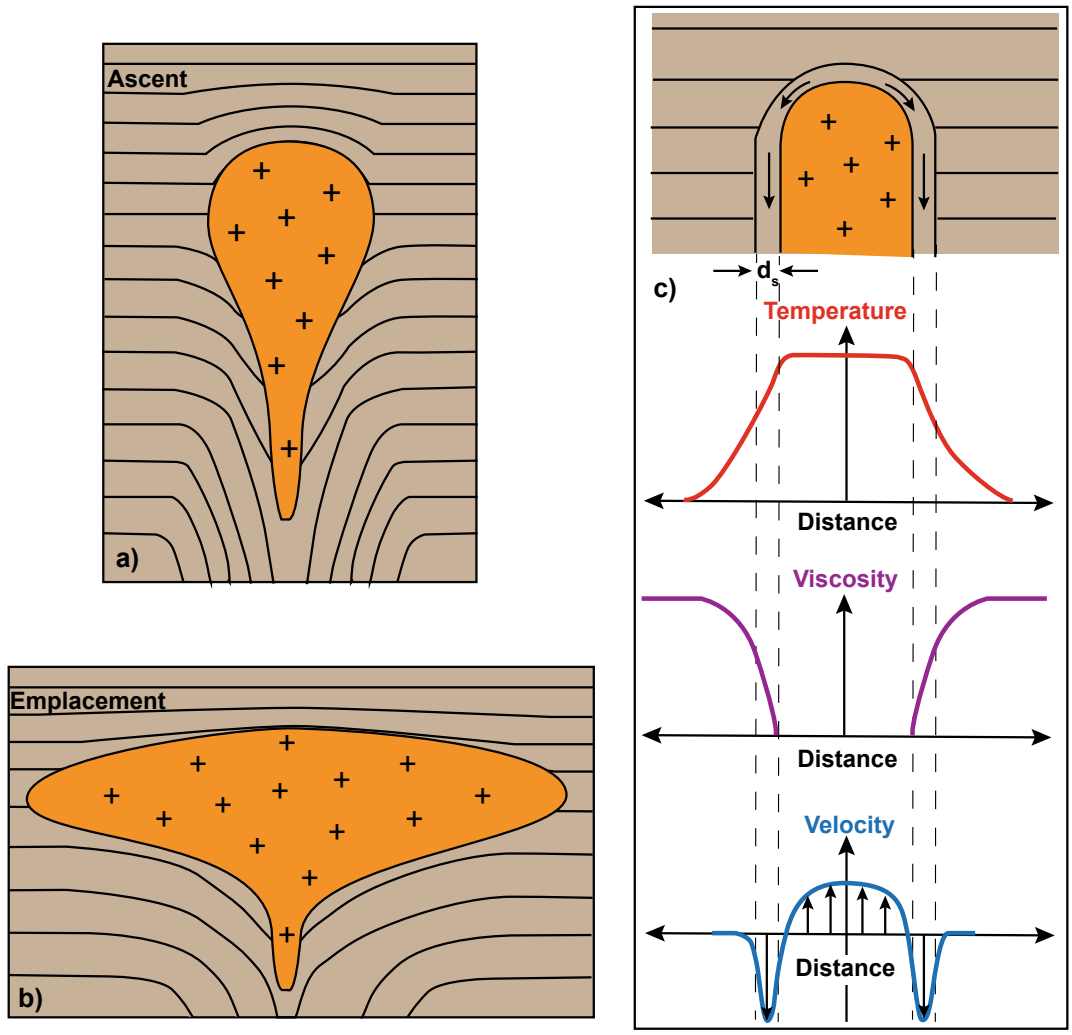


**Fig. 3.1** Section view scheme of a **a** rising magmatic diapir, resembling an inverted teardrop, and an **b** emplaced diapir, attaining a mushroom-like shape, **c** temperature, viscosity and velocity variations within the top part of a rising diapir and the country rock; $d_s$ = thickness of softened region (modified after Marsh 1982)

$$t = \frac{13.04\eta}{(\rho_1 - \rho_2)gT_u} \tag{3.1}$$

where $\eta$ is the viscosity of both fluids, $\rho_1$ and $\rho_2$ are the densities of the upper and lower layer, respectively, and $g$ is the acceleration due to gravity (e.g., Turcotte and Schubert 1982). Equation 3.1 indicates that the more viscous the fluids and the smaller their density difference, the longer it takes to grow an instability.

The initiation of an instability develops a diapir flowing upwards, which becomes progressively taller and narrower. The diapir rises within the country rock, eventually becoming detached from its root and acquiring an inverted tear-drop shape, with wider domed head and narrower tail.

### 3.2.2 Diapir Rise

The ascent rate of a magmatic diapir may be derived from the Stokes' law, although the common assumption of the isoviscous

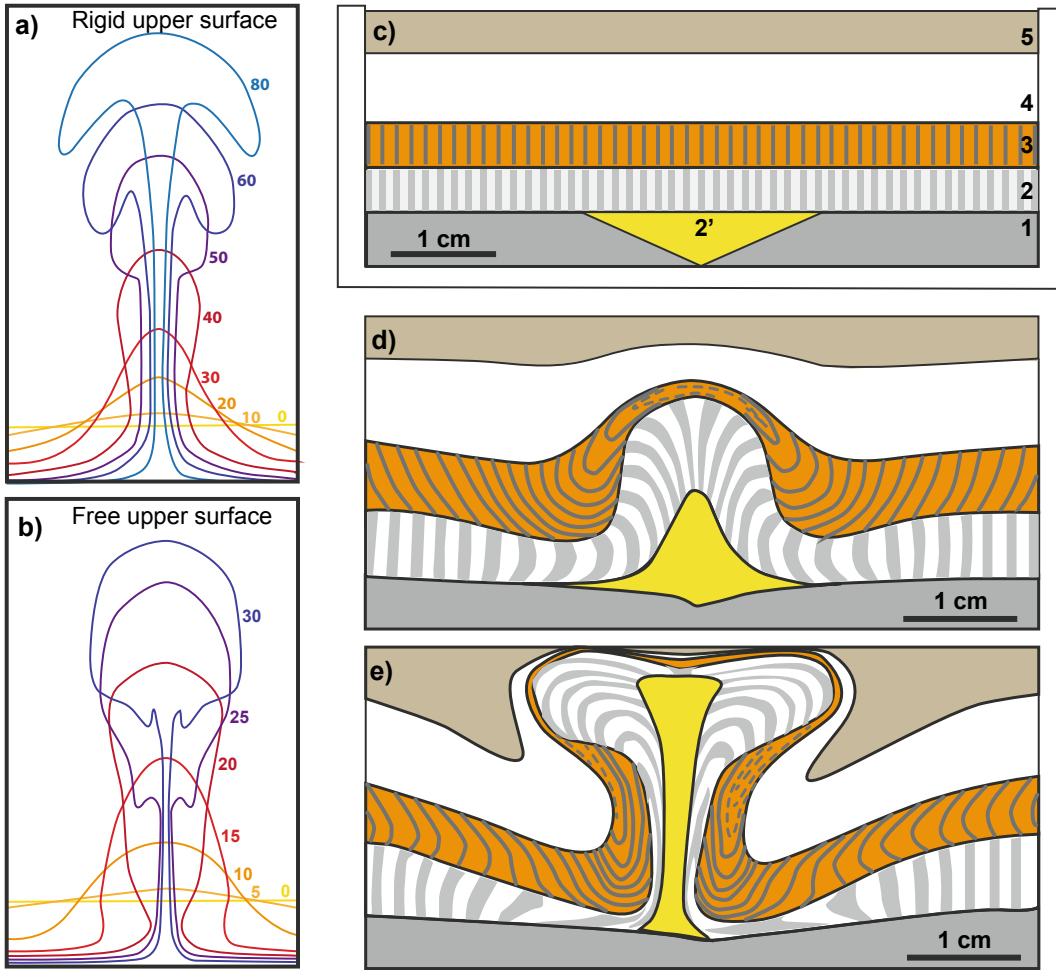


**Fig. 3.2** **a**, **b** Numerical experiments of rising magmatic diapirs, showing the section view shape of diapirs at different times, in seconds, with different boundary conditions: rigid upper surface (**a**) and free upper surface (**b**), the latter with rise about twice fast. In both cases, the width of the diapir first decreases and then increases (Berner et al. 1972). **c**–**e** Centrifuge experiments (at 2000 g) of rise of lighter viscous material (1400 kg/m$^3$; layers 2 and 2′) into denser viscous material (1480–1560 kg/m$^3$; layers 3, 4 and 5); **c** schematic section view of the model before deformation; **d** section of model after 310 s in the centrifuge; **e** section of model after 505 s (Ramberg 1981)

surrounding medium of the latter may not be appropriate for a hot diapir inducing a thermal gradient within the country rock. In fact, the ascent rate and extent of the diapir are strongly dependent on the width of the deformation layer (with thickness $d_s$ in Fig. 3.1) of variable viscosity that is formed by the transfer of heat to the country rock and on the buoyancy force which propels the diapir through it. In particular, the ascent velocity $U_a$ is described by the expression:

$$U_a = \frac{2\Delta\rho g d_s^3 Z_v}{\eta r} \tag{3.2}$$

where $\Delta\rho$ is the density contrast between the diapir and the country rock, $g$ is the acceleration due to gravity, $d_s$ is the deformation zone width,

$Z_v$ is a parameter which describes the increase in viscosity across the zone, $\eta$ is the country rock viscosity at the contact, and $r$ is the diapir radius (Marsh 1982; Mahon et al. 1988). Equation 3.2, which leads to the definition of the "hot Stokes model", shows that the ascent velocity varies with the diapir size, with larger bodies moving more slowly and ascending for longer periods relative to smaller bodies. Also, the ascent velocity of a diapir is inversely proportional to the viscosity of the surrounding medium, which should be less than $10^{15}$–$10^{16}$ Pa s to ensure diapir rise. Although a single diapir would have difficulty penetrating through a highly viscous region in the crust, once a conduit has been established by the previously hot rising magma, the resulting viscosity decrease of the country rock may promote diapiric transport through an otherwise less permeable medium. The ascent distance of the magma depends on the rheology and ambient temperature of the encompassing rock and on the initial diapir temperature, which determines the amount of released thermal energy. Because of the proportionately larger amount of available thermal energy, larger bodies will rise greater distances.

The relationship between growth rate of amplitude and time highlights a sigmoidal pattern, characterized by an exponential slow-growth phase, a linear rapid phase and an exponential stationary phase, defining an overall S-like shape. The final volume of the diapir is acquired at the beginning of the linear rapid phase of growth, implying reduced alimentation from the trunk in the later phase. The growth rate depends on the degree of melting and the volume of the magma, as well as on its viscosity (Berner et al. 1972; Bittner and Schmeling 1995).

In the case of isoviscous surrounding medium (or even of a thin envelope characterized by thermal softening outside the diapir), the rise of the diapir is accompanied by the progressive flattening and rotation of material above and the progressive stretching below, identifying the domains represented in Fig. 3.3 (Cruden 1988).

In particular, the diapir roof is gently dipping and unfaulted, overlaid by flat lying roof strata. Towards the diapir margin these strata surrounding the diapir roll over into a steeply dipping **rim synform**, or annular downward closing fold, resulting from the viscous drag forces related to gravitationally driven roof collapse and

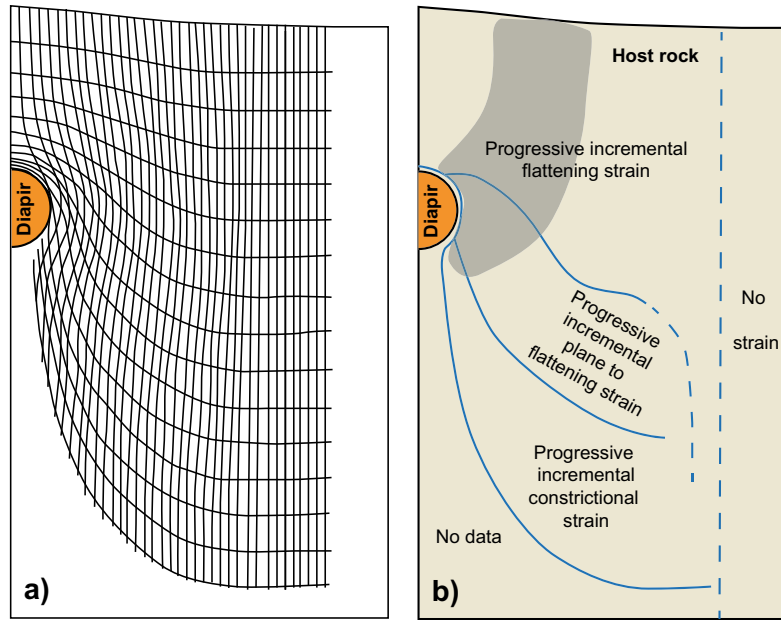


**Fig. 3.3** **a** Reconstruction of the deformation within markers in a fluid to the side (half image) of a sphere simulating a rising diapir within ductile crust. **b** Map showing regions of progressive incremental strain in the fluid passing the sphere; grey shaded area highlights the region where the rotational component of deformation is significant (>70% of rotation; modified after Cruden 1988)

channel flow along the diapir margins (see the velocity profile in Fig. 3.1; England 1992; Paterson and Farris 2006). In the field, rim synforms are commonly observed at mid-crustal levels, to the sides of eroded Cordilleran plutons, where the strain due to the rim synform on the diapir margin is expected to increase with depth. This suggests widespread downward transport of country rock during pluton emplacement, involving important volumes of material and ultimately contributing to crustal thickening (Paterson and Farris 2006).

### 3.2.3 Diapir Emplacement

The emplacement of a diapir occurs when the diapir stops ascending. In a first approximation, the emplacement depth depends on the buoyancy, size and temperature of the diapir. The buoyancy depends on the **Level of Neutral Buoyancy** (LNB), that is when the intrusion density $\rho_m$ equals the country rock density $\rho_r$ (see also Eq. 1.2). A magma lighter than the country rock ($\rho_m < \rho_r$) has positive buoyancy and will tend to rise; conversely, a denser magma ($\rho_m > \rho_r$) has negative buoyancy and will tend to sink. As the density of the Earth generally increases with depth, a same magma may be positively buoyant at the base of the crust and negatively buoyant near the surface (Fig. 3.4). As for the diapir size, small diapirs (<5 km in diameter) with minor density contrast with regard to the country rock ($\sim 100$ kg/m$^3$) are expected to stall in the lower crust. Large diapirs (>5 km in diameter) and with significant density contrast ($\sim 400$ kg/m$^3$) may rise to shallower levels, possibly even faulting the overlying rocks (Burov et al. 2003). As for the temperature, the hotter the magma, the lower its viscosity and the easier is the flow of the diapir within the crust; a hotter magma is also lighter, increasing its buoyancy; finally, the hotter the magma, the softer is the surrounding deformation layer, further enhancing the rise of the diapir through the country rock.

The level of emplacement of a diapir also depends on the physical state of the country rock. In fact, if the strength of the country rock becomes significantly larger than the force promoted by buoyancy, a diapir may stop its ascent and start to emplace even before reaching any level of neutral buoyancy. This condition is commonly met in correspondence of the brittle-ductile transition, whose depth mainly depends on the geothermal gradient, the strain rate and the

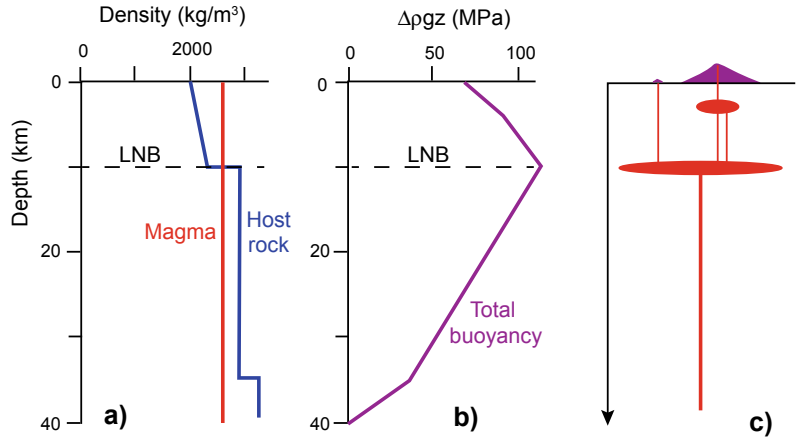


**Fig. 3.4** Buoyancy force acting on a magma column in a stratified lithosphere. **a** Variation of density with depth; **b** variation of total magmastatic head with depth; **c** at the Level of Neutral buoyancy (LNB) magma may accumulate and differentiate in "hot zones," from where shallow crustal reservoirs are supplied (modified after Gonnermann and Taisne 2015)

tectonic setting: here the strength of the crustal rocks dramatically increases, hindering the further rise of diapirs (see Sect. 3.2.5; Bateman 1984; Bittner and Schmeling 1995). The depth of emplacement of a diapir also depends on the rheological behaviour of the ductile crust around it. In fact, diapirs are inferred to rise faster and emplace at shallower levels through a power law (non-Newtonian) crust than through a Newtonian crust, and such faster rise is not accompanied by the large heat loss expected with Newtonian crust. This behaviour results from the decrease in the effective viscosity, and thus resistance, of the non-Newtonian crust, which promotes strain rate softening (Weinberg and Podladchikov 1994).

When the diapir emplaces, its rate of growth decreases significantly, while its rate of crystallization increases. During emplacement, the diapir head spreads laterally, attaining a mushroom-like shape. This growth is propelled by the rise of the still positively buoyant main body and tail of the diapir. Eventually, the ~10% increase in the density of an emplaced diapir during final crystallization may promote its foundering within the country rock, particularly if the latter is rich in low density minerals (quartz, calcite). This possibility is supported by field evidence showing rim anticlines (i.e., annular upward closing folds) surrounding several plutons, as in the Great Basin of western North America (Glazner and Miller 1997).

Recognizing emplaced diapirs in the field is not straightforward, as other types of intrusions may be commonly mistaken for diapirs. This is the case of magmatic "balloons" produced by **ballooning**, which is the in-situ (at the level of emplacement), radial expansion (without predominant direction of movement) of an intrusion or magma chamber. In the common ballooning model, magma ascends until loss of heat or buoyancy causes the outermost magma to crystallize and cease ascent, while the hotter magma tail continues to rise and expand the already crystallized outer margin. This expansion forms a concentric, flattening-type strain in the pluton periphery and pushes aside the surrounding country rock, a process which may take hundreds of thousands of years (Fig. 3.5). This process may be encouraged by regional tectonic activity. For example, shortening at the base of the pluton may squeeze the magma upwards, causing expansion at higher crustal levels and promoting ballooning (Bateman 1985; Ramsay 1989; Rosenberg et al. 1995).

There are many similarities between balloons and diapirs. Both are subcircular in map view,

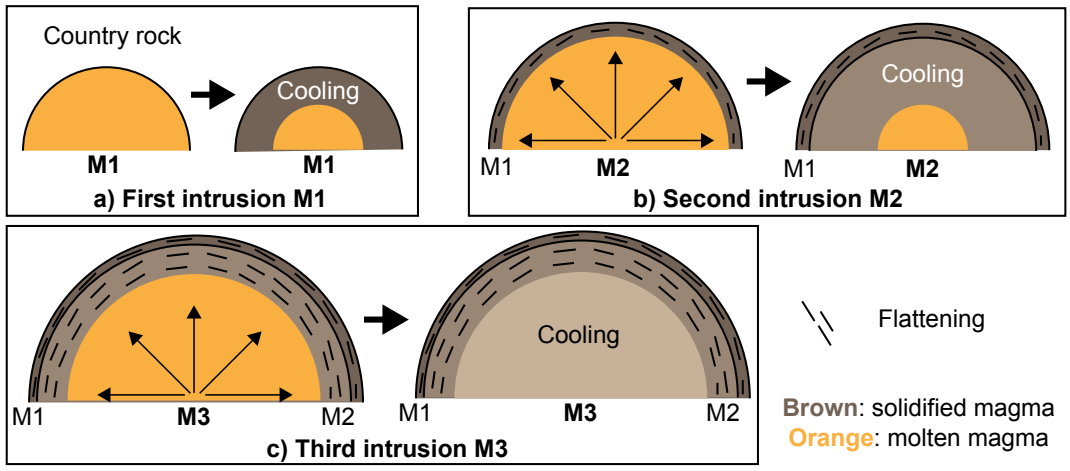


**Fig. 3.5** Possible development of a composite intrusion through ballooning, section view. After a first intrusion M1, partially solidified (brown part, **a**), a second inner intrusion of magma M2 pushes away and flattens the outer shell of the first intrusion (**b**); when the second intrusion is solidified, a third inner intrusion M3 emplaces and flattens the shell of the first and second injections, eventually solidifying (**c**; modified after Ramsay 1989)

with concentric fabric and concentrically deformed wall rocks, with the strain increasing toward the pluton contact. However, a few differences do exist (e.g., Paterson and Vernon 1995). In diapirs, magma ascent may occur by rise of large magma batches, instead of transport in dikes followed by emplacement and ballooning. More importantly, the evaluation of the predominant direction of movement of the intrusion relative to the country rock may allow distinguishing balloons from diapirs. Ballooning is the radially directed expansion of a body in situ with no predominant movement: hence, while balloons should show no pluton-up kinematics, diapirs should be associated with pluton-up kinematics, and steep, well-developed lineations. Therefore, a balloon has not moved unidirectionally from its point of inflation, whereas a diapir can only be satisfactorily recognized if it has risen more than one body diameter. In other words, diapirism can be proven beyond doubt where it is possible to demonstrate uplift of country rock in excess of the vertical thickness of the intrusion. However, this requires accurate knowledge of the three dimensional shape of the intrusion and its country rock, a condition which is rarely met, resulting in an overall difficulty to demonstrate any diapiric ascent (England 1990; Molyneux and Hutton 2000). The difficulty in distinguishing diapirs from balloons can be also overcome identifying marker deflections in the field. These are useful for evaluating country rock displacements during diapirism or ballooning, provided that either the pre-emplacement geometry of the markers is known, or that rigid rotations and stretches are known (Paterson and Fowler 1996).

Using these approaches, several field studies recognized eroded portions of magmatic diapirs, usually with granitoid compositions (Ramsay 1989; Galadi Enriquez et al. 2003; He et al. 2009). These include the Chindamora granitic batholith (Zimbabwe), built by magmatic pulses at more than 15 km depth and also showing important ballooning, or the La Bazana granite (Spain), with a teardrop–pipe shape suggesting lateral expansion and vertical flattening, emplaced at 7–10 km of depth. The Cretaceous Fangshan granodiorite pluton (North China) has a bulk wall-rock shortening by ductile flow of ~4 km, similar to the pluton radius, and a rim synform formed during the late-stage rise of the diapir, emplaced at a depth of 3–6 km (Fig. 3.6). A rim synform is also found around the Northern Arran Coarse Granite (Scotland; England 1992). These cases suggest that diapirism may be a viable mechanism for the migration and emplacement of magma up to 5–10 km in depth, depending on the local conditions.

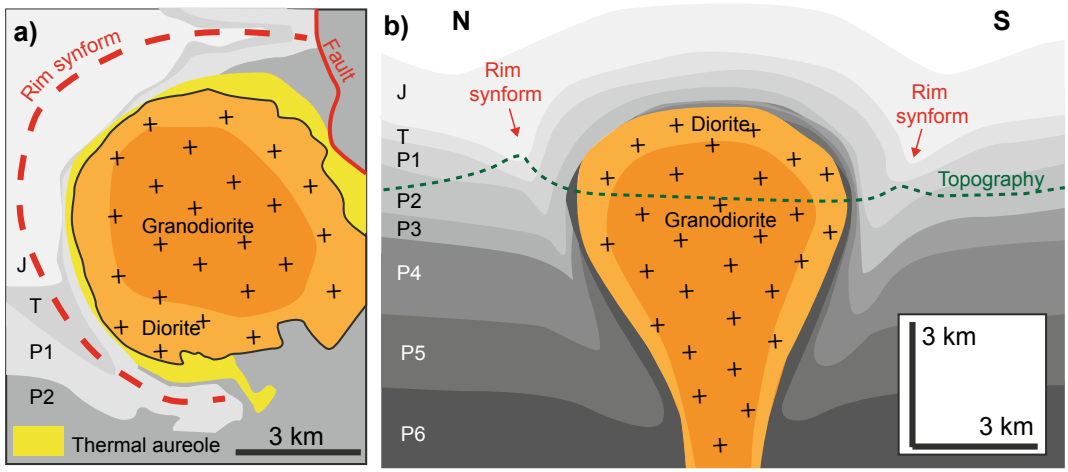


**Fig. 3.6** Map **a** and schematic section view (**b**; approximately N–S) of the eroded Fengshan diapir (China), associated with a rim synform to the side (modified after He et al. 2009)

There is also indirect evidence of ongoing diapir emplacement, as suggested by the tens of kilometres wide uplifted area surrounded by a broader zone of subsidence in the Altiplano-Puna region of the Central Andes. This specific deformation pattern is inferred to result from the emplacement of a mid-crustal diapiric magma body at ~20 km of depth, although this interpretation is debated (Fialko and Pearse 2012; Henderson and Pritchard 2013).

### 3.2.4 Diapirism and Stoping

The rise of diapirs is often accompanied by magmatic stoping. **Stoping** consists of disconnecting and surrounding a piece of country rock (namely, the thermal halo) by magma, moving blocks relative to their position prior to emplacement (Fig. 3.7).

Stoped blocks may be displaced downward (sinking) or, less commonly, upward (floating), depending on their density contrast with the magma. Stoping is a process through which the magma essentially mines its way upward, and it is not limited to diapirs. Stoping may in fact occur also along magma chamber roofs, sides, and floors, at any crustal level, and blocks may form through a number of different processes, as thermal cracking, diking, tectonic stresses and focused porous flow (Marsh 1982; Paterson et al. 2008). Thermal cracking is possibly the easiest means to promote stoping at the top of voluminous magmatic intrusions. Here the heat of the intrusion causes expansion of the country rock, producing tensional stresses and developing cracks. The stresses required for fracturing necessitate only moderate changes in temperature, on the order of 100 °C, implying limited energy transfer. A model alternative to thermal shattering has been proposed for the development of stoped blocks in the Cordilleran batholith of Oregon (USA). Here stoping is seen as a multi-stage process involving the emplacement of sills along bedding planes and formation of short connecting dikes cutting across bedding. This results in a sill–dike network enclosing rectangular roof blocks along the batholith–roof contact (Zak et al. 2012). A further model has related stoping to short-lived roof collapse events in active magma chambers: accordingly, stoped blocks may record collapse of the roof during large caldera-forming eruptions (Hawkins and Wiebe 2004).

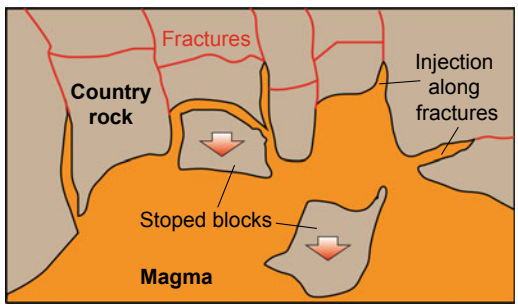


**Fig. 3.7** Scheme illustrating the mechanism of stoping, where fractures at the top of a magmatic intrusion promote injection of magma and subsequently the foundering of the blocks surrounded by the fractures within the magma

Stoping requires the rate of advance of the diapir be determined by the rate of removal of blocks from its roof, while the ascent distance is probably limited to a few body heights, because stoped blocks rapidly congest the magma. Although stoping does not make space, it can facilitate magma ascent by vertical mass exchange. Field evidence from plutons cited in favour of stoping includes the following: (a) sharp, discordant contacts between plutons and wall rocks; (b) a lack of pluton-related ductile deformation of wall rocks; (c) xenoliths in plutons, also from diverse sources; (d) geochemical evidence for magma contamination (Glazner and Bartley 2006).

The importance of magmatic stoping has been debated, with studies considering it unlikely to be a volumetrically significant process and others highlighting it to be widespread in all types of plutons, where it may account up to 20% or the observed magma mass. Several field studies support this latter view, considering magmatic stoping as a dominant process of downward transport of country rock in upper crustal plutons, or of magma evolution also in the middle and lower crust (Dumond et al. 2005; Zak and

Paterson 2006; Glazner and Bartley 2008; Paterson et al. 2008; Yoshinobu and Barnes 2008). Indeed, there is much to be gained by studying stoping with regard to high-temperature rheological behaviour and magma emplacement, as stoped blocks may provide information about paleohorizontal during emplacement of plutons and about the timing, kinematics and magma viscosities during fabric formation (Paterson and Miller 1998a).

### 3.2.5 Limitations of Diapirism as a Mechanism for Magma Transport

Until the 1990s, diapirism was a very popular mechanism to explain the rise of magma, with the main limitation that a diapir, unless being very large (with a small surface area to volume ratio) would soon run out of heat and hence rise only short distances in the crust (Marsh 1982). This limitation has been partly relaxed considering a ductile crust with power law behaviour, encouraging the faster and shallower rise of diapirs and limiting the large heat loss inferred to occur with a Newtonian crust. A further limitation inferred for the rise of diapirs has been due to the crystallinity of magma. While the rise of crystal-rich magma is generally enhanced by diapirism, with significant crystallization (>70%) diapiric ascent is prevented and any further magma injection may inflate the diapir through ballooning (Bateman 1985).

Studies in the 1990s highlighted a further and crucial limitation for diapirism, underlining the inadequacy of the diapiric ascent of magma through buoyancy in the upper brittle crust. In particular, magma buoyancy increases with the density contrast with the country rock and with the height of the magma column (Fig. 3.8a; Paterson and Farris 2006). For example, assuming a density contrast between the magma ($\sim$2400 kg/m$^3$) and surrounding crust ($\sim$2750 kg/m$^3$) of $\sim$350 kg/m$^3$ leads to a buoyancy force of $\sim$3.5 MPa per 1 km of height of magma. Such a value is two orders of magnitude less than the stress value required to

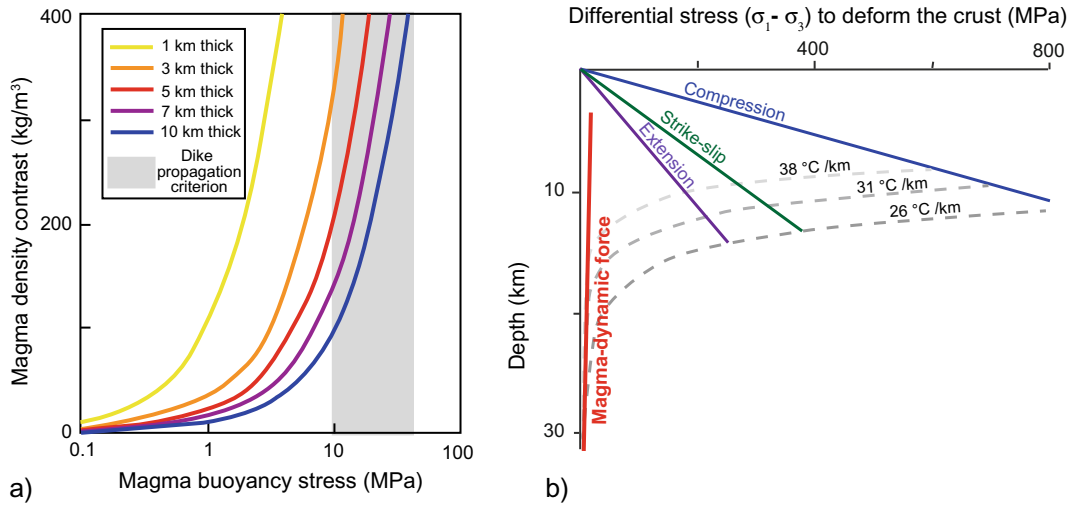


**Fig. 3.8** **a** Plot of magma/country rock density contrast and buoyancy stress for magma columns of varying height. Thin (1 km thick) plutons generate small buoyancy stresses. Magma columns of more than 5–10 km high and density contrasts larger than 100–200 kg/m$^3$ are needed to propagate dikes and initiate wall rock fractures from buoyancy stresses alone. The grey area indicating the dike propagation criterion is from Jellinek and DePaolo (2003) (modified after Paterson and Farris 2006). **b** Schematic rheological profile showing the variation in the crustal strength as a function of the tectonic setting and geothermal gradient. The dynamic force of a magma column starting at the Moho (red line) shows that this does not match the differential strain required to break the brittle crust (modified after Vigneresse 1995)

penetrate the brittle-ductile zone at a depth of approximately 10 km, that is on the order of a few hundred of MPa (Fig. 3.8b; Vigneresse 1995).

The discrepancy between the force caused by the buoyancy of the magma and the differential stress required to fracture the brittle crust remains high even assuming a lighter magma incorporating an important percent of fluid phase. Only an unrealistically tall column of diapiric magma (hundreds of km) would overcome the shear resistance of the crust by buoyancy. This implies that, at the brittle-ductile transition zone, the buoyancy force of a magmatic diapir becomes insufficient to fracture the upper brittle crust and the magma cannot rise further only by buoyancy. The brittle-ductile transition should be thus considered as the upper limit of penetration of magmatic diapirs. However, this transition should not be perceived as a fixed barrier, as its depth is affected by the thermal and mechanical state (i.e., pre-existing fractures) of the crust. For example, repeated magma emplacement, also through diapirs, may progressively heat the crust, shallowing the brittle-ductile transition and the emplacement level of magmatic diapirs (Cao et al. 2016).

Finally, the diagram in Fig. 3.8b also shows that the strength required to break the brittle crust is about four times larger under compression than under extension. This implies that the easiest condition for magma to intrude the brittle crust is within extensional tectonic settings, where the stress level is lowest. Nevertheless, extensional volumes may be found also in localized zones within strike-slip or contractional settings (see Sect. 4.5.2 and Chap. 10; Vigneresse 1995).

## 3.3 Magma-Filled Fractures

Diapirs may be a viable means for the rise of magma in the crust although, because of the limitations discussed in the previous section, they are likely not the predominant mode, especially at shallow levels. In fact, dikes provide the main mode of rise of magma within the crust, at any level. Dikes, with inclined sheets and sills, are **magma-filled fractures**, or subplanar intrusions whose thickness is much smaller than their vertical or lateral extent. In particular, **dikes** are magma-filled fractures discordantly cutting at high angle across layers, **sheets** are magma-filled fractures discordantly cutting at moderate angle across layers, and **sills** are magma-filled fractures concordant with the country rock layers (Fig. 3.9). As a consequence, in presence of horizontal or poorly-tilted layers, as in active volcanic areas, dikes are usually subvertical, sheets are inclined and sills subhorizontal. These terms are used for both the actively propagating magma-filled fractures and the solidified intrusions. In this section the emphasis is on magma-filled fractures, whereas the following sections of the chapter focus on the general principles of dike propagation and arrest within the crust. Sills, as mainly responsible for magma emplacement and accumulation, and often anticipating the development of magma chambers, are considered in Chap. 4; dike nucleation from magma chambers is also considered in Chap. 4. The shallower propagation of dikes and, to a lesser extent, sheets and sills within volcanoes and the implications for eruptive activity are described in Chap. 7.

Magma-filled fractures are much thinner than their length and width: their usual thickness is on the order of metres, while the typical length and width is on the order of kilometres, or more. This leads to aspect ratios on the order of $10^{-3}$ to $10^{-4}$. Even though magma-filled fractures are often assumed to be planar or subplanar, they may exhibit deviations from planarity, both along strike and dip.

Dikes ensure the transfer of magma at any crustal level, also feeding eruptions from shallow magma chambers. Such a transfer may be characterized by predominant vertical propagation, responsible for the rise of magma, or predominant lateral propagation, transferring magma away for tens of kilometres and eventually feeding distal eruptions outside volcanoes. Conversely, sills are usually responsible for the emplacement and accumulation of magma in the crust, especially at shallow levels (few km of depth), although in several cases sill systems

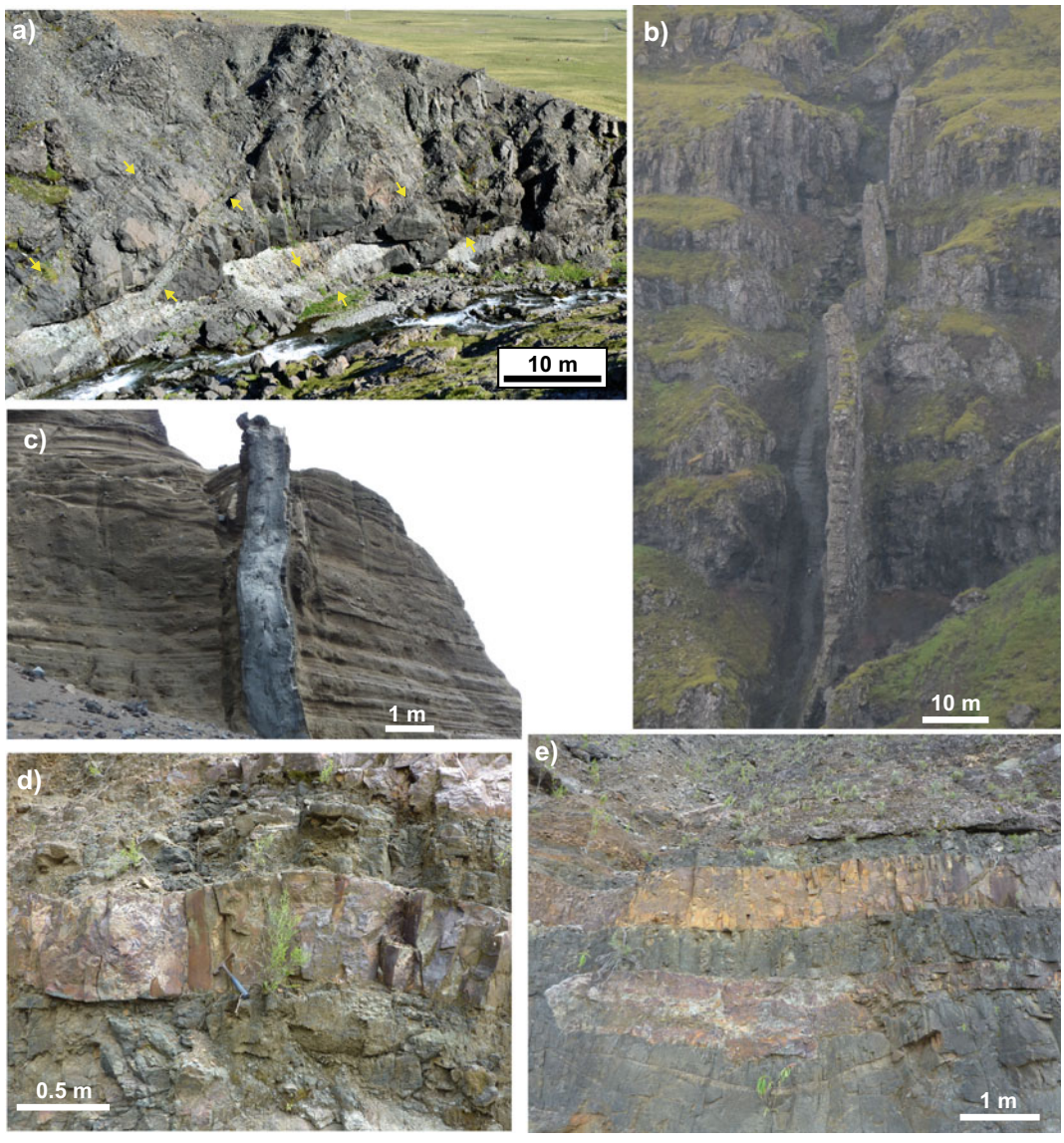


**Fig. 3.9** Field examples of magma-filled fractures. **a** Series of inclined sheets (highlighted by the yellow arrows) intruded in a succession of sub-horizontal Tertiary lava flows; the intrusions belong to the Midhyrna-Lysuskard cone sheet system, Snaefellsnes Peninsula, northwestern Iceland (Photo courtesy: Alessandro Tibaldi). **b** Three en-echelon dike segments observed in an eroded portion of a rift zone in eastern Iceland. **c** A feeder dike outcropping in the Capelinhos Peninsula, site of the last eruptive activity (1957–1958) in Faial (Azores). A portion of a sill **d** and a set of stacked sills **e** observed at Piton des Neiges, La Reunion Island; note the blunt left termination of the lighter reddish sill in the lower part of **e**

have been responsible for relevant lateral magma propagation. Also, while dikes can propagate independently of pre-existing fractures (see Sect. 3.5), sill formation is often enhanced in correspondence of pre-existing subhorizontal anisotropies, as layering or fractures (see Sect. 4.3). In between, sheets may transfer and/or emplace magma in the crust, mainly depending upon their dip and the characteristics of the country rock (as far-field stress, anisotropies).

An important feature common to all magma-filled fractures is that, to ensure propagation and

thickening, these tend to develop perpendicular to the least principal stress $\sigma_3$. Therefore, the plane approximating the magma-filled fracture contains the maximum and intermediate principal stresses $\sigma_1$ and $\sigma_2$, although their exact plunge cannot be determined from the orientation of the magma-filled fracture alone. Because of this, from a dynamic point of view magma-filled fractures behave as extension fractures. When the emplacement of magma-filled fractures results from far-field (regional, or tectonic) stresses, subvertical dikes are expected to form in extensional or strike-slip settings, where the least principal stress $\sigma_3$ is horizontal, and subhorizontal sills are expected to form in compressional settings, where the least principal stress $\sigma_3$ is vertical (Fig. 3.10).

Significant deviations from this simple behaviour may occur if far-field stresses are overprinted by any near-field (local) stress, as induced by important topographic variations, magmatic sources, layering, fractures or other features. For example, the development of inclined magmatic sheets requires an inclined least compressive stress $\sigma_3$ and thus non-Andersonian conditions. The latter are usually inhibited by far-field stresses and promoted by near-field stresses, as those developed by magma chambers. Therefore, the presence and orientation of dikes, sheets or sills at a given place within the crust ultimately depends on the combination of both the far-field and near-field acting stresses. The stress conditions for the development of dikes and sills, with the respective vertical $\sigma_v$ and horizontal $\sigma_h$ stress components, which may result from any far- and/or near-field stress, are reported in Fig. 3.11 (Jaeger 1969; Gressier et al. 2010). For both dikes and sills the magmatic pressure reduces the normal stresses, but not the deviatoric stress. The Mohr circle thus shifts leftward and, if it touches the failure envelope, fracturing occurs. In an anisotropic medium, characterized for example by layering, sill formation depends on the deviatoric stress and the tensile strength parallel and perpendicular to the layering.

Magma-filled fractures are expected to form and grow with low viscosity magmas, as with mafic and low viscosity felsic compositions. In fact, high viscosity felsic sheets will be likely halted by freezing soon after the magma encounters rock at temperatures below the magma solidus (Emerman and Marrett 1990; Rubin 1995a). Magma composition may also affect the geometry of magma-filled fractures, as revealed by estimates of the viscosity of several dikes in different tectonic settings, which show that dike thickness increases with magma viscosity (Wada 1994). In particular, mafic magmas with viscosities of $10^1$–$10^2$ Pa s tend to form metres-thick dikes, while felsic magmas with viscosities of $10^6$–$10^7$ Pa s tend to form thicker dikes. Therefore, magma viscosity, as determined by its composition, appears an important factor to explain the thickness variations in dikes.

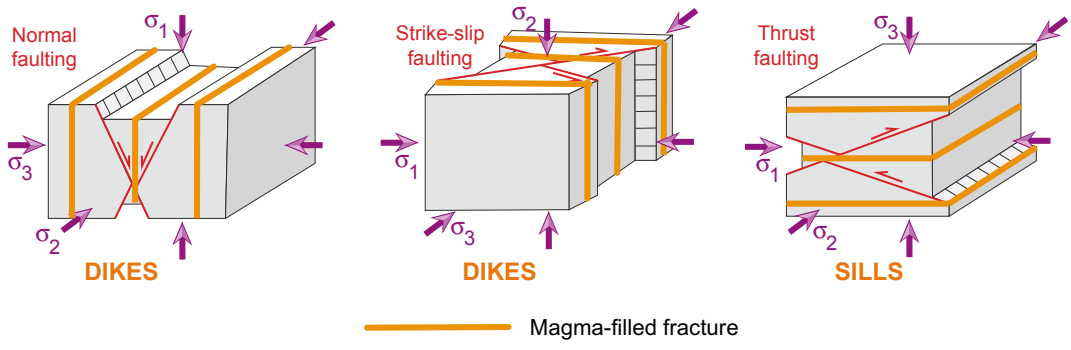


**Fig. 3.10** Types of magma-filled fractures (dikes and sills) expected to develop as a function of the regional tectonic regime. Inclined sheets, not included here, are commonly induced by the local stress field induced by a magma chamber

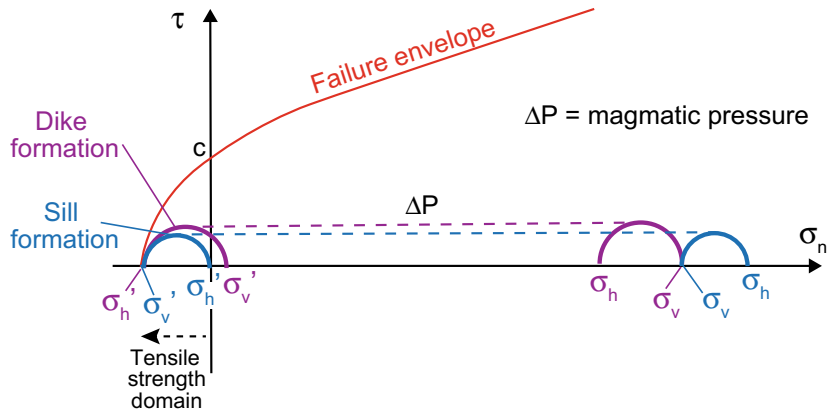


**Fig. 3.11** Mohr Coulomb diagram illustrating the stress conditions for the development of dikes (purple) and sills (blue). These conditions refer to a zone in the country rock at the tip of a propagating dike or sill. The magmatic pressure $\Delta P$ shifts the Mohr circles to the left, passing from a vertical $\sigma_v$ and horizontal $\sigma_h$ to $\sigma_v'$ and $\sigma_h'$, allowing the propagation of sills and dikes (modified after Gressier et al. 2010)

Independently of their orientation, magma-filled fractures, developing perpendicular to the least principal stress $\sigma_3$, share overall similar mechanisms and conditions of formation and propagation. These mechanisms and conditions are described below in the case of dikes, although with minor modifications they may be extended to sills and sheets.

## 3.4 Dike Propagation

As this chapter discusses the rise of magma, this section focuses on the general case of dike propagation within the crust, neglecting the mechanism of dike nucleation from magma chambers, which is considered in Sect. 4.6.3.

Dikes are responsible for the transfer of magma at any crustal level, as well as within volcanic edifices, where they feed eruptions. Indeed, most eruptions are fed by dikes. This holds not only for eruptive fissures, for monogenic fields, or for eccentric vents on the volcano slopes, but also for summit craters fed by a central conduit in polygenic volcanoes. The importance of dikes in building central conduits is underlined by observations at several volcanoes, including drilling data at Unzen felsic stratovolcano (Japan), which indicate that the same central conduit consists of a dike swarm (Sakuma et al. 2008). For these reasons, understanding dike propagation is crucial to define shallow magma transfer and to ultimately forecast eruptions (see also Chap. 9).

Dikes can be approximated as magma-filled cracks with overall ellipsoidal shape. Their reported thickness to length aspect ratios are usually between $10^{-2}$ and $10^{-4}$ (Fig. 3.12). Dikes can propagate anywhere within the crust, with velocity on the order of m/s, without suffering the limitations mentioned in Sect. 3.2.5 for magma rising through diapirs. Dikes in fact focus the forces required for magma ascent at their tips, where these become much larger than the fracture resistance of the country rock. Because in situ tensile strengths of typical country rocks of dikes and sheets are approximately 0.5–6 MPa, the theoretical crack-tip values of dikes are from 100 to 10,000 times greater than the tensile strength of country rocks (Lister and Kerr 1991; Gudmundsson 2002). Also, dikes can propagate not only vertically, but also laterally and, at times, even with a downward component along the slope of a volcano or in the crust. The substantial independence of the dike propagation direction from the direction of gravity is a further factor that distinguishes dike ascent from diapirism and from porous flow in the source region of magma (Rubin 1995b).

**Fig. 3.12** Subvertical dikes with variable thickness observed along the south coast of Tenerife (Canary Islands); the white boats provide a scale

Dike formation and propagation have been commonly investigated focusing on the deformation processes within the country rock (the "solid mechanics" approach) or on the viscous flow of magma within ("fluid mechanics" approach). Both approaches are considered below.

### 3.4.1 Solid Mechanics

The growth of a dike involves both elastic (associated with the thickening of the dike along its length) and inelastic (of limited extent, mainly fracturing at the dike tip) processes within the country rock. Therefore, excepting the tip region, deformation of the country rock is assumed to be largely elastic, and this motivates treating dikes as cracks in a linear elastic body. Let us first consider the elastic behaviour of the country rock. For uniform loading stresses, the thickness profile of a dike is elliptical and its half-thickness $w$ at the centre is assumed to be (Fig. 3.13; Rubin 1995b, and references therein):

$$w = \frac{P_e}{E_s} L \tag{3.3}$$

with

$$P_e = P - \sigma_n \tag{3.4}$$

and

$$E_s = \frac{G}{1 - v} \tag{3.5}$$

being $L$ the half-length of the dike, $P_e$ the **magmatic excess pressure**, given by the difference between the internal magma pressure $P$ and the ambient compressive stress perpendicular to the

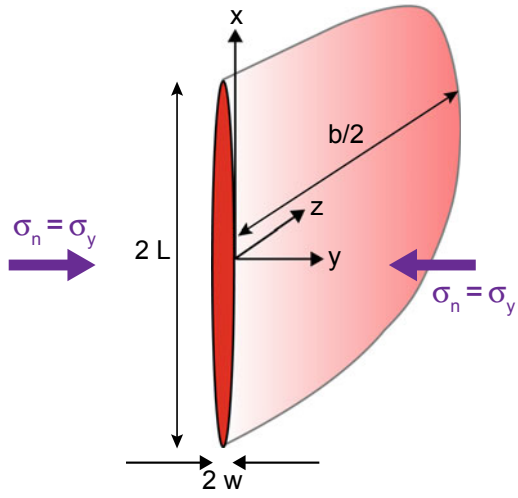


**Fig. 3.13** Schematic view of dike of length $2L$ (along the direction of propagation), width $b$ and thickness $2w$ experiencing a normal pressure $\sigma_n$ on its walls

dike plane $\sigma_n$, and being $E_s$ the elastic stiffness of the country rock, determined by its elastic shear modulus $G$ and Poisson's ratio $v$. Considering that the in situ elastic stiffness $E_s$ is on the order of a few tens of GPa or less, and observing in the field the length and thickness of outcropping dikes, Eq. 3.3 can be used to estimate the related excess pressures: these are on the order of a few to $\sim$10 MPa, although considerable variation is expected.

Equation 3.3, despite of its wide applicability, provides a simplified approach, as non-elastic processes may also control dike thickness. Recent field studies on thin dikes (thickness < 1 m) show that these are relatively thick at their ends and narrow in the middle, with shapes poorly matching the elastic theory. These shapes can be explained by country rock inelastic deformation and magma chilling at the dike tips, which prevent closure as magma pressure declines (Fig. 3.14; Daniels et al. 2012). While the application of these results to thicker dikes is not straightforward and requires further investigation, other studies confirm the importance of non-elastic processes in constraining dike thickness. These studies, based on thousands measurements from dikes in different tectonic settings, suggest that the country rock lithology, in particular the strength as defined by material defects and fracture toughness, is a dominant factor in controlling dike thickness (Krumbholz et al. 2014).

As for the inelastic behaviour occurring at the dike tips, it is useful to distinguish three regions: the crack, where the country rock is completely separated; the intact country material, where deformation is essentially elastic; the region in between surrounding the crack tip, or "process zone", where the strength of the material has been exceeded, but where inelastic deformation has not proceeded to develop a crack. The criteria commonly used to analyse the propagation of the fractures at the dike tip consider the local stress or the energy balance (Rubin 1995b, and references therein). In the first case, if there is no macroscopic crack and the material experiences uniaxial tension, the appropriate fracture criterion is that at the dike tip the tension due to the magmatic pressure exceeds the tensile strength of the material. If the material is under compression, the tensile failure criterion postulates that the

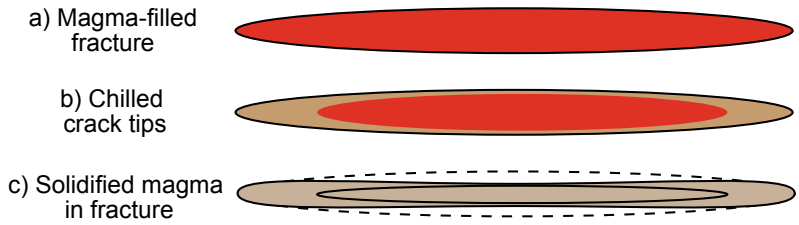


**Fig. 3.14** Scheme showing the impact of cooling on dike geometry. **a** Magma creates a dike (section view); **b** cooling ensues at the dike margins (brown portions); **c** complete solidification creates the observed dike profile (outer solid line), with thinner centre and thicker tips with regard to an expected profile of a pressurized magma-filled fracture in elastic medium (the latter is exemplified by the dashed line; modified after Daniels et al. 2012)

magmatic pressure at the dike tip exceeds the least compressive stress by some tensile strength (Fig. 3.11). If a macroscopic crack exists, the stress concentration at the tip allows propagation to occur at a lower applied tension or magmatic pressure. The second case considers dike propagation to occur when the associated release of potential energy is sufficient to provide the energy required for fracturing at the tip. This potential energy consists of elastic strain energy, plus any work done on the country rock. In particular, dike propagation occurs when the potential energy release per unit increase in dike length equals the critical value required for propagation. Linear Elastic Fracture Mechanics (LEFM) provides a useful framework for this approach, quantifying the stress required to propagate a fracture and using the notions of crack-tip stress intensity factor $K$ and rock fracture toughness $K_c$.

The **stress intensity factor** is used to describe the stress intensity near the tip of a crack: all else being equal, the longest crack has the highest stress intensity factor (see Sect. 2.5). **Fracture toughness** is the property that describes and quantifies the ability of a material to resist fracture. The fracture toughness of a material is determined from the stress intensity factor at which a thin crack in the material begins to grow. Thus, at the onset of crack propagation, the fracture toughness becomes the critical stress intensity factor, so that crack propagation occurs when $K = K_c$ (Lister and Kerr 1991; Rubin 1995b). The stress intensity factor $K$ is a fundamental component of the stress field near the crack or dike tip. While $K$ depends upon the crack size and applied forces, being

$$K = P_e\sqrt{L} \tag{3.6}$$

for a uniformly pressurized bladelike fracture of size 2 $L$ under pure tensile failure (Mode I crack), $K_c$ is a material property that can be experimentally defined, usually being on the order of 1 MPa $m^{1/2}$ and increasing with pressure. If $K$ slightly exceeds $K_c$, the dike (or a crack) will propagate and magma will flow toward the tip. The propagation of magma within the fracture is thus described by Eq. 3.6, substituting $K_c$ to $K$. However, magma cannot flow too fast, or the associated drop in pressure (see Sect. 3.4.2) toward the tip would drop $K$ below $K_c$. Therefore, the propagation speed of a dike is limited by the fracture toughness. If $K < K_c$, the dike may propagate very slowly, only by chemical corrosion at its tip.

### 3.4.2 Fluid Mechanics

The fluid mechanics approach focuses on the flow of magma within the dike and at its tip. In this approach it is usually sufficient to consider the magma flux averaged over the channel thickness, assuming laminar flow. For laminar flow, the velocity is zero at the dike walls and varies parabolically across the channel thickness. Laboratory experiments also indicate that crystal- and bubble-free magmas may be treated as Newtonian viscous fluids.

Near the dike tip the average flow velocity in the propagation direction approaches the tip velocity. Here the magma decreases its pressure, attaining a value $P_t$ before reaching the narrow crack tip, and a gap, or **tip cavity**, forms between the tip and the magma front (Fig. 3.15; Lister and Kerr 1991; Rubin 1995b, and references therein). This low pressure region results from the dynamical difficulty of forcing a viscous fluid to flow into a thin gap. The tip cavity is mainly filled by the volatiles exsolving from the magma, as its low pressure promotes exsolution even when the dike is well below the level at which the magma would normally become saturated. Examples of relict tip cavities include cracks extending beyond the magma front in a dike and pegmatite zones at the tips of granitic dikes. The dike tip experiences underpressure, or tip suction, defined as $P_s = P_t - \sigma_n$. The greater the tip suction, the shorter the tip cavity, while the larger the dike, the larger the tip cavity. In a first approximation, as the tip cavity has limited extent with regard to the dike size, it also has limited control on its thickness and velocity of propagation. Therefore, the existence of the tip cavity can be ignored in most calculations

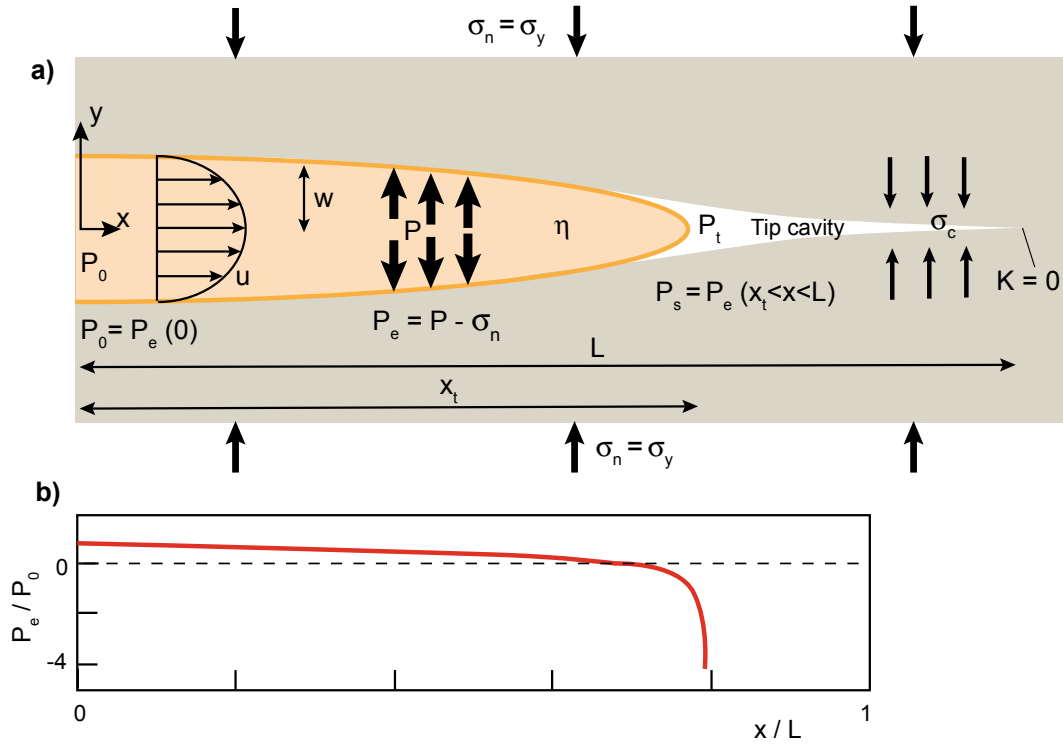


**Fig. 3.15** **a** Two-dimensional not to scale scheme of propagating dike, with emphasis on the tip region. Material properties: magma viscosity $\eta$, cohesive stress $\sigma_c$ acting over the critical crack-wall separation. Boundary conditions: ambient dike perpendicular compression $\sigma_n$ (or $\sigma_y$), magma pressure at dike entrance $P_0$, magma pressure P, magma excess pressure $P_e$, pressure at tip cavity $P_t$, tip suction $P_s$, dike half-thickness w, position of magma front $x_t$, average flow velocity $u$. Propagation criterion is $K = 0$ at tip of cohesive zone. **b** Computed excess magma pressure $P_e$ within the dike, normalized by $P_0$, as referring to **a** (modified after Rubin 1995b)

dealing with dike propagation. Nevertheless, the tip cavity may play a fundamental role in promoting inelastic deformation, and thus seismicity, at the dike front. Behind the tip cavity lies the bulbous nose of the dike, with maximum thickness some 25% greater than $2w$ (Fig. 3.16a; Lister and Kerr 1991; Rubin 1995b). This swollen zone results from the impossibility to have magma underpressure along the main walls of the dikes, as suggested by calculations. In fact, if the dike narrowed monotonically towards the tip, the pressure gradient for flow would also increase monotonically, generating the underpressure along the dike; conversely, an increased thickness at the head of the dike implies a reduced pressure drop along the dike.

Generally three sources of pressure may promote magma flow in dikes and contrast the viscous resistance to flow: the excess magma pressure at the source, the magma buoyancy and the differential stress acting on the dike. These three contributions define the driving pressure, or **magmatic overpressure** $\Delta P_m$, responsible for magma flow in a dike, which is expressed as (Gudmundsson 1990; Rubin 1995b; Gudmundsson et al. 1999):

$$\Delta P_m = P_e + (\rho_r - \rho_m)\, g\, h + \Delta\sigma \qquad (3.7)$$

where $P_e$ is the magmatic excess pressure above the lithostatic pressure (resulting for example from magma addition, gas exsolution), $h$ is the vertical distance from the magma source chamber and $\Delta\sigma = \sigma_v - \sigma_h$ is the difference between the vertical $\sigma_v$ and the horizontal $\sigma_h$ far-field principal stresses. Usually, for dike propagation

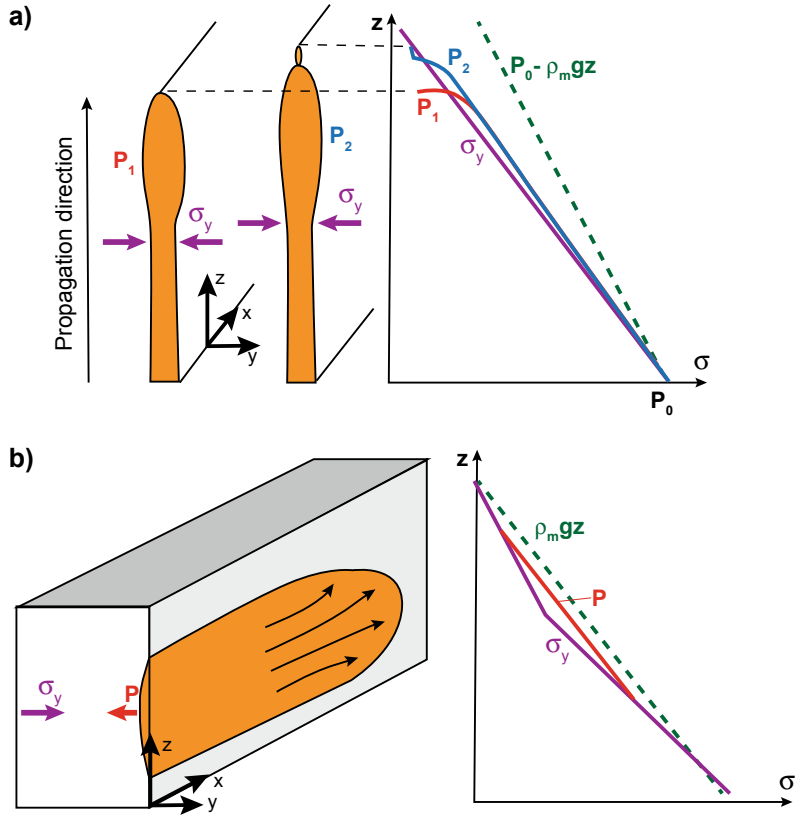


**Fig. 3.16** **a** Scheme showing two stages of vertical propagation of a dike. Magma pressures $P_1$ and $P_2$ deviate from ambient dike-perpendicular stress $\sigma_y$ only over a certain length below tip. Dashed green line represents the static magma pressure curve, with $P_0$ being the magma pressure at dike entrance. At stage 1 (left cartoon), tip suction is large and tip cavity is small; at stage 2 (right cartoon), magma front is closer to volatile saturation depth and tip cavity may become unstable. **b** Scheme showing the lateral propagation of a blade-like dike from a shallow source. The related stress state required for lateral propagation is shown in the right diagram. The kink in $\sigma_y$ may be due to a density step or to variations in tectonic stress (modified after Rubin 1995b)

the horizontal stress is the minimum principal stress $\sigma_3$, while the vertical stress is the maximum principal stress $\sigma_1$: therefore, $\Delta\sigma$ may be commonly approximated by the deviatoric stress. Equation 3.7 thus indicates that the magmatic overpressure increases with the following conditions. (a) "Internal" loading (magma-related), as increasing the magmatic excess pressure, for example by adding magma or exsolving gases. (b) "External" loading (country rock-related), as increasing the deviatoric stress by decreasing the $\sigma_3$ component, as for example under extension. (c) The interaction between internal and external factors (the density difference, or buoyancy), as injecting lighter magma in denser crustal rocks.

As the overpressure $\Delta P_m$ in a vertically propagating dike also increases with the dike length $L$, once the dike grows sufficiently that $(\rho_r - \rho_m)gh > P_e$, magma buoyancy begins to provide the dominant pressure gradient for flow. In addition to increasing its length, during the early stages of propagation the dike also widens along the direction parallel to its strike, or width. Once the dike has reached a critical width driven by its elastic and buoyancy pressures, it does not widen further, due to the finite fracture toughness of the country rock. The dike will then predominantly lengthen at a rate governed by a balance between its viscosity and buoyancy (Fig. 3.16a; Gonnermann and Taisne 2015).

As at intermediate to great crustal depths the country rock density usually exceeds that of the magma, buoyancy is an important contribution in Eq. 3.7. At shallow crustal depths, however, rocks have densities similar to that of the magma. The density of the country rock immediately above the magma chamber may be even less than that of the magma, making it more difficult for the magma to rise through buoyancy alone. When a dike reaches the Level of Neutral Buoyancy (LNB) of the magma, it may stop ascending: if this occurs, magma may propagate laterally through dikes or sills, depending on the stress field. The requirement for the lateral propagation of a dike is that the excess pressure at the dike centre exceeds that at the dike top and bottom and, at the same time, shows a lateral gradient (Fig. 3.16b; Lister and Kerr 1991; Rubin 1995b). The condition for lateral magma propagation has been commonly referred to in the literature as related to the LNB. Nevertheless, recent experimental studies significantly relax the importance of buoyancy in the lateral propagation of dikes, rather highlighting the importance of rigidity layering (a stiffer layer overlying a weaker one) and topography (see Chap. 7; Urbani et al. 2018). Also, the filter role of the LNB on magma ascent is relaxed by three possible conditions promoting an additional rise of a dike above the LNB. (a) Degassing, which may further decrease magma density in the dike, providing some additional buoyancy (Gudmundsson et al. 1999). (b) The fact that the local **magmastatic pressure** gradient $(\rho_r - \rho_m)g$ does not need to be positive everywhere in the dike: it needs to be positive only when averaged over the dike length. Therefore, magma could be erupted in a negatively buoyant upper crust, provided that there is a sufficiently large underlying region in which the magma is positively buoyant (Fig. 3.4). (c) The elastic stress build-up due to magma accumulation at the LNB may also cause an overshoot beyond the LNB through a vertical distance depending upon the dike width and the supply rate from below. The same overshoot may also drive the magma laterally along the LNB (Lister and Kerr 1991). These results are generally confirmed by numerical results, which show that the velocity of a vertically propagating dike initially increases with the dike length, reaches a peak when the dike tip is well above the LNB and then rapidly decreases to zero after the dike propagates further into the region above (Chen et al. 2011). Nevertheless, numerical calculations of dike propagation through layered rocks emphasize that penetration through low density rocks is determined by the local buoyancy only in the swollen nose region, rather than the total buoyancy of the magma column integrated from the source to the tip (Taisne and Jaupart 2009). This feature may strengthen the filtering role of the LNB.

If both the density and the far-field stress terms in the right side of Eq. 3.7 approach zero or become negative (for example at shallow crustal levels and in compressional settings), the initial excess pressure becomes the only driving pressure of the dike. Because of the pressure drop due to viscous drag, the excess pressure may also soon fall to zero and the vertically propagating dike becomes arrested. In fact, while the flow of magma in a dike is driven by a gradient in the fluid pressure, a main force contrasting dike propagation is the pressure drop in the magma due to its viscous resistance to flow. The **viscous pressure drop** $\Delta P_d$ in laminar flow along the length $2L$ of a dike with magma viscosity $\eta$ in a time $t$ since the initiation of the dike is estimated as (Lister and Kerr 1991):

$$\Delta P_d \approx \frac{\eta 4L^2}{w^2 t} \tag{3.8}$$

If the flow is turbulent, Eq. 3.8 underestimates the viscous pressure drop. However, magma flow in thin dikes is likely to be laminar, and most treatments of magma flow within dikes approximate the flow as one-dimensional, laminar, and incompressible. As concerns magma flow, the mean velocity of magma $U_d$ with pressure P within the dike propagating along the $x$ direction (see Fig. 3.13) averaged across the dike thickness is (Rubin 1995b):

$$U_d = -\frac{1}{3\eta} w^2 \frac{dP}{dx} \tag{3.9}$$

This allows defining the **volumetric flow rate** $Q_f$ of a vertically oriented dike as:

$$Q_f = -\frac{b}{3\eta} w^3 \frac{dP}{dx} \qquad (3.10)$$

where $b$ is the dike breadth or width, which is the dimension perpendicular to the direction of propagation ($x$) and to the half-thickness $w$ of the dike (Fig. 3.13). Thus, the volumetric flow rate of magma into a dike is inversely proportional to magma viscosity and proportional to the dike thickness cubed. This relationship implies an expected time delay, on the order of hours to days for basalts and years for granites, before an incipient dike tip becomes sufficiently pressurized to propagate (Gonnermann and Taisne 2015). The focusing (i.e., channeling) of magma from a linear dike to a central eruptive vent fed by the dike just below the surface is also a consequence of the strong cubic dependence of flow rate on dike thickness expressed by Eq. 3.10. Because most of the flow becomes channelled along the thicker sections of the dike, the rate of magma cooling during ascent will be lowest there, perhaps even promoting melting or erosion of the dike walls. In contrast, thinner sections of the dike will have lower flow rates and faster rates of magma cooling. This will increase the viscosity of the magma, as well as its solidification along the dike walls. The overall result is a progressive reduction of the portion of the dike actively feeding flow, as also discussed in Sect. 7.7.

As the propagation velocity of dikes driven by excess source pressure is inversely proportional to the magma viscosity, dikes filled by viscous magma could also produce significant viscous deformation of the country rock. Under common conditions of excess magma pressure and elastic stiffness of the country rock, the magma-country rock viscosity contrast must exceed 11–14 orders of magnitude for the viscous contribution to dike thickness to be negligible. These large contrasts are met by all basalts and most granites (Rubin 1993). However, very viscous granites (viscosity $\eta \geq 10^8$ Pa s) might have lower viscosity contrasts with regard to hot crustal portions, so that the viscous displacements along the dike wall away from the tip can exceed the elastic displacements by 1–2 orders of magnitude. In this case, a viscous deformation of the country rock occurs. Nonetheless, the resulting intrusions are still narrow, with thickness to length ratios expected to be no larger than $10^{-2}$: in fact, even in this case elastic strains continue to dominate near the tip. These theoretical predictions are confirmed by experimental studies and field observations. In particular, experiments suggest that the aspect ratios of dikes around the brittle–ductile transition approach diapir–dike hybrids deviating from dikes in an elastic medium (Fig. 3.17; Sumita and Ota 2011). In the field, an exhumed dike complex in the Scandinavian Caledonides records increasing ductile features (dikes with rounded shapes and mingling between the soft country rock and the intruding mafic magma) approaching the paleo brittle-ductile transition (Kjoll et al. 2019). Similarly, intrusions in the Cascades (northwest North America) and in the North American Cordillera emplaced at depths between 10 and 30 km show a vertically elongated shape, with length to width

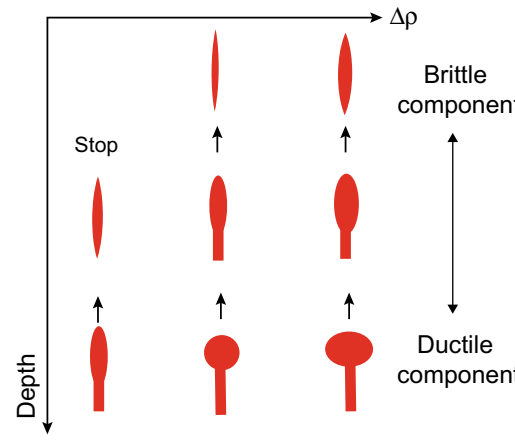


**Fig. 3.17** Schematic diagram showing how magma may change its shape as it ascends through the brittle-ductile transition zone. Here three cases for a same magma volume, but different density difference $\Delta\rho$ are shown (modified after Sumita and Ota 2011). Diapir–dike hybrid intrusions may occur at intermediate crustal depths, consistently with what observed in the field

ratios <100, surrounded by country rock deforming by visco-elastic processes, and for which ascent is driven by buoyancy plus regional stress. These features suggest that hybrid mechanisms of ascent, involving both a diapiric and a diking component, are common at mid-crustal levels (Paterson and Miller 1998b; Miller and Paterson 1999).

### 3.4.3 Thermal Constrains

The above discussion neglects the influence of the temperature on the rheology of the magma and country rock. However, because dikes carry hot magma into colder rock, heat flow must be an important aspect of magma intrusion: while freezing of magma might prevent dikes from erupting, melting of the country rock might alter the composition and properties of the magma. The understanding of the thermal aspects of dike propagation is probably less advanced than that of the mechanical aspects, and only an overview is given here.

Magma cooling and/or solidification and melt against the dike walls are a consequence of the conduction of heat from the magma into the dike walls. The degree to which magma cools depends on the balance between along-dike heat transport by the flowing magma (which depends on the magma propagation velocity) and the across-dike diffusion of heat to the conduit walls (which depends on the gradient in temperature across the magma within the thermal boundary layer close to the dike walls). The ratio between these two competing heat transfer mechanisms leads to the dimensionless parameter $\Pi$ (Bruce and Huppert 1989; Gonnermann and Taisne 2015):

$$\Pi \approx \frac{w^4 \Delta P}{\alpha \eta 4 L^2} \tag{3.11}$$

where $\Delta P/2L$ is the average pressure gradient driving magma flow within the dike and $\alpha$ is the thermal diffusivity. For small half-thickness of the dike $w$, magma cooling dominates. Cooler magma will increase the viscosity, which will reduce magma velocity and pressure, implying a further decrease in heat transfer through the dike relative to conductive heat loss to the dike walls. The result will be flow localization, that is, sections of the dike with small $\Pi$ tend to close. Conversely, sections with large $\Pi$ remain open (Fig. 3.18; Gonnermann and Taisne 2015, and references therein). In particular, during dike propagation a thermal boundary layer develops closest to the dike walls, where heat transfer is dominated by conduction, as opposed to along-dike convection by magma flow. When the thermal boundary layer thickness is much less than the dike thickness, the frozen margin thickness $w_f$ grows with time as:

$$w_f = 2\lambda(\alpha t)^{1/2} \tag{3.12}$$

where $\lambda$ is a numerical coefficient which depends upon the initial magma and country rock temperatures, the freezing temperature, the latent heat of crystallization and the heat capacity $C_p$ (Carslaw and Jaegar 1959; Rubin 1995b, and references therein). The time taken for a dike to

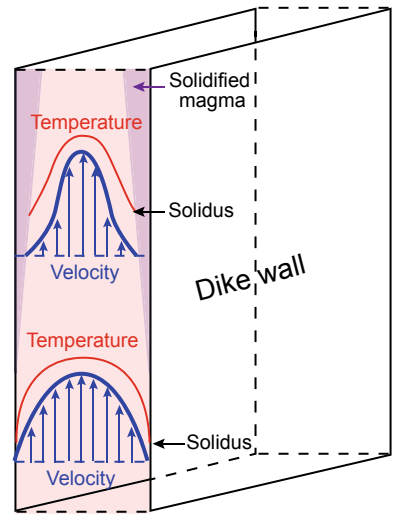


**Fig. 3.18** Scheme illustrating the evolution of the velocity and temperature profiles for magma ascending within a dike. As the magma cools against the conduit walls (purple wedges, upper part), viscosity increases and velocity decreases, reducing the heat transport, resulting in a positive feedback between cooling, increasing viscosity and decreasing velocity (modified after Gonnermann and Taisne 2015)

completely solidify is given by (Lister and Kerr 1991):

$$t = \frac{w^2}{\lambda\alpha} \tag{3.13}$$

The short duration of heat transfer (on the order of hours) and small temperature increase (well below that of the magma) in the country rock during the emplacement of a dike under ordinary conditions explain the lack of contact metamorphic (i.e., heating) effects next to many dikes (Delaney and Pollard 1982). An estimate of the distance that dikes may propagate before freezing is given by multiplying the solidification time (Eq. 3.13) by the flow velocity (Eq. 3.9). The resulting propagation distance $L_p$ can be expressed as (Rubin 1995b):

$$L_p = \frac{1}{12\lambda^2}\frac{w^4}{\alpha\eta}\frac{dP}{dx} \tag{3.14}$$

where $\eta$ is the magma viscosity and $dP/dx$ is the variation in magma pressure along the direction of propagation of the dike. These results show that a dike cannot propagate beyond a critical length, which may be estimated as order of magnitude by Eq. 3.14. More precise estimates are mainly limited by the difficulty in calculating the numerical coefficient $\lambda$ deriving from models that incorporate both the mechanics of propagation and the thermodynamics of solidification. Considering these limitations, applying this equation to a rhyolite four orders of magnitude more viscous than a basalt suggests that the rhyolite dike would have to be ten times thicker in order to propagate as far. This implies that dikes filled with mafic magma commonly have critical thickness of a very few metres, one order of magnitude lower than that of dikes filled with granitic magma (Lister 1995).

### 3.4.4 Seismicity Constraints

The propagation of dikes and, more generally of any magma-filled fracture, is usually responsible for seismicity. Indeed, the generated earthquakes often represent the strongest evidence for dike propagation, allowing to constrain dike geometry, kinematics and dynamics, and carrying a wealth of information on the physics of diking. Dike seismicity is briefly considered here to further define the mechanism of propagation of dikes in the upper crust.

Magma emplacement commonly stresses the nearby country rock; these stresses create the fractures and faults which are ultimately responsible for the generation of earthquakes. In particular, most dike-induced seismicity, with frequency typical of tectonic earthquakes, should be interpreted as resulting from slip along suitably aligned existing fractures to the sides of the dike. Dike-induced earthquakes typically have minor to moderate magnitude, not exceeding 6. As a result, the seismicity associated with dike propagation lacks the higher magnitude spectrum typical of tectonic earthquakes. Observations from the 1975–1984 rifting episode at Krafla (Iceland) first highlighted that propagating dikes induce migrating seismicity. However, the migration of seismicity does not necessarily reflect the migration of the dike. Rather, the seismicity is linked to the evolution of the stress field associated with the opening of the dike and to the stress previously stored in the crust. Therefore, the distribution of the recorded dike-induced seismicity reflects the distribution of ambient stresses that are near to failure and does not necessarily reflect the true extent of the dike. This implies that seismicity can also occur on a different time scale to the migration of the dike tip. While the data often hint at a broad equivalence between tip migration and seismicity, there is evidence that the tip is not the only and at times not even the primary source of seismicity (Rubin and Gillard 1988; Rivalta et al. 2015; Amhed et al. 2016). Despite such a possible independence between the extent of a dike and the distribution of its seismicity, studies on several intrusions also highlight a proportional relationship between the average thickness of a dike and the mechanical energy released by its propagation. This feature may help predicting the total seismic moment that will be released by a propagating dike once its thickness is constrained by geodetic data (Bonaccorso et al. 2017).

In the case of a laterally propagating dike, models and observations show that when seismicity is at intermediate depth between the dike top and bottom, earthquakes focus at the leading edge of the dike. Then, as the dike tip advances and the seismogenic volume falls into a stress shadow, seismicity stops. Conversely, when seismicity is above or below the dike, it continues at a decaying rate after the dike tip passes (Segall et al. 2013). While both space–time patterns have been observed in nature, seismic observations from recent diking events in different tectonic settings reveal some additional variability in the earthquake distribution during dike propagation, where even similar events may show important changes. For example, there is a marked difference between the seismicity associated with the lateral propagation of tens of kilometres long dikes emplaced between 2007 and 2009 at Dabbahu (Afar) and that in 2014 at Bardarbunga (Iceland). At Dabbahu the seismicity focused at the lateral tip and at the top of the propagating dikes, with the largest magnitude earthquakes generated by normal faulting above the dikes (Grandin et al. 2011; Belachew et al. 2013). Conversely, at Bardarbunga seismicity focused at the bottom of the propagating dike tip, with earthquakes showing evidence of both left- and right-lateral faulting behind the leading edge of the dike (Fig. 3.19; Agustdottir et al. 2016; Woods et al. 2019).

The kinematics of the faults responsible for seismicity can be detected through the focal mechanisms of the earthquakes, which describe the deformation in the source region (for details see Sect. 8.4.1). Both Dabbahu and Bardarbunga diking events show a consistent pattern of focal mechanisms along the tip of the dike, generally coherent with a local maximum principal stress $\sigma_1$ directed outwards along the propagating dike tip and a local minimum principal stress $\sigma_3$ perpendicular to the propagating tip of the dike. This stress distribution broadly results in seismicity characterized by normal focal mechanisms, ideally forming conjugate normal faults, on the top of the dike, and by dextral and sinistral mechanisms, ideally forming conjugate strike-slip faults, to the sides of the laterally propagating dike tip (Fig. 3.20).

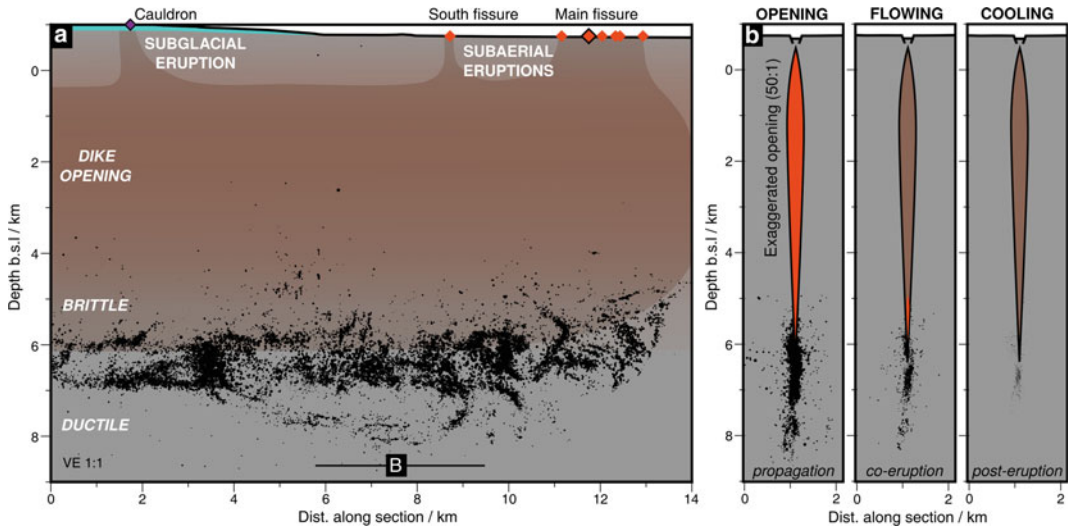


**Fig. 3.19** Seismicity of the 2014 Bardarbunga (Iceland) fissure eruption. **a** Dike-parallel cross-section with schematic dike opening shaded and **b** dike-perpendicular cross-section with interpretative cartoon for propagation, eruption and post-eruption phases. Black dots show relocated dike-induced earthquakes. Ice cauldron indicated by dark purple diamond; eruption fissures shown as orange diamonds. (Courtesy of Jennifer Woods; Woods et al. 2019)

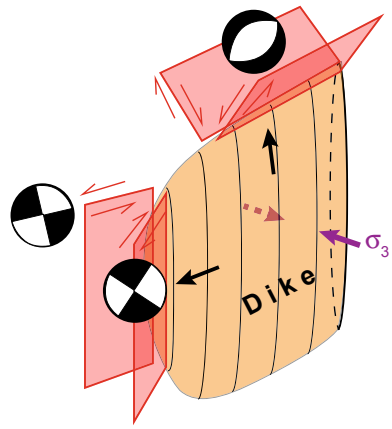


**Fig. 3.20** Scheme not to scale summarizing the main fault systems (red rectangles) and seismicity (focal mechanisms highlighted by the beach balls seen in map view; see Sect. 8.4.1 for details) induced at the upper and lateral tips of a propagating dike (orange; local sense of propagation shown by black arrows). Conjugate normal faults predominate on the top of the dike, as observed at Dabbahu (Afar, Ethiopia), whereas conjugate strike slip-faults predominate to the sides, as observed at Bardarbunga (Iceland)

Other diking events presented common features to Dabbahu and Bardarbunga: these include the laterally propagating dike in Miyakejima (Japan) in 2000, with strike-slip events at the front of the shorter dike edge, normal fault events along the upper dike edge and the whole range of intermediate kinematics between these types. Similarly, the dikes propagating at Aden in 2010–2011 and the Southern Red Sea in 2011 induced seismicity with focal mechanisms indicating predominant normal faulting to the front and above the dikes (Passarelli et al. 2015; Amhed et al. 2016; Eyles et al. 2018). In addition to fault-related (double-couple) mechanisms, the seismicity associated with dike emplacement may also involve a fluid related (non-double-couple) component, indicating faulting mechanisms deviating from pure shearing and including a tensile component (see Sect. 8.4.1).

Focal mechanisms may provide information not only on the orientation, shape and pressurization level of the dikes, but also on any variation of these parameters. For example, the study of focal mechanisms associated with diking has allowed obtaining the stress variations before, during and after eruptive events. In the case of the 1992 eruption at Mount Spurr (Alaska, USA), the seismicity highlighted a rotation of the stress field related to the pressurization of a network of dikes, with stress changes corresponding to changes in the state of activity at the volcano (Fig. 3.21a; Roman et al. 2004). In particular, the NE–SW direction of the maximum principal stress locally revealed by the earthquakes prior to the eruption was perpendicular to the NW–SE regional maximum principal stress. After the eruption, the former rotated of $\sim 90°$, becoming parallel to the regional maximum principal stress. A few months later, during a seismic swarm induced by a magmatic intrusion, the local maximum principal stress rotated, assuming again a NE–SW orientation. Finally, in the years after the eruption, the stress direction was again parallel to the NW–SE regional stress. This horizontal rotation of the maximum principal stress likely resulted from the pressurization of a system of interconnected dikes, promoting stress increase in the country rock to the sides of the dikes responsible for seismicity. This feature is consistent with theoretical predictions, as in absence of mechanisms for relaxing the stresses due to intrusions, repeated dike emplacement can raise the dike-perpendicular stress until it is no longer the least principal stress, causing future sheet intrusions to take the form of sills or dikes of opposite orientation (Fig. 3.21b; Rubin 1995b; Vigneresse et al. 1999; Xu and Jonsson 2014).

Some aspects of the patterns of dike-induced seismicity are still poorly understood, as the temporal distribution of seismicity at the inferred advancing and retreating fronts of migrating epicentres of a laterally propagating dike. In fact, an advancing front, usually shown by a convex-upward trend in the case of lateral migration, is commonly trailed by a retreating front delimiting a frame of active seismicity (Fig. 3.22; Rivalta et al. 2015). While the advancing front has generally a simple shape, the retreating front may show a more complex pattern, with variable distance with regard to the advancing front.

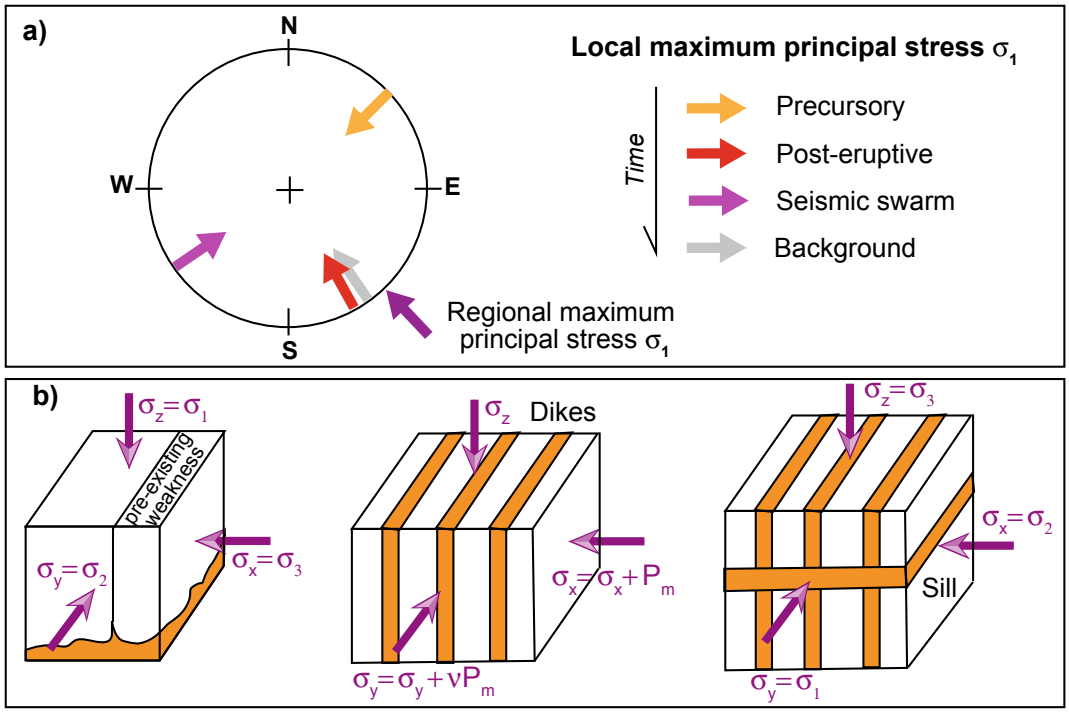


**Fig. 3.21** **a** Stereograph showing the orientation of the local maximum principal stress at Mount Spurr (Alaska, USA) during four defined periods with regard to the regional maximum principal stress (modified after Roman et al. 2004). **b** Scheme of stress axes exchange under the influence of magma intrusion in extensional conditions: (left) initially, the opening plane is vertical (*yz*; forming a dike) and perpendicular to the minor stress component ($\sigma_3$); (centre) due to the pressure of magma intrusion ($P_m$), the minor stress increases to $\sigma_3 + P_m$, whereas the intermediate axis increases proportionately to the Poisson coefficient ($\nu$); (right) provided the two horizontal components overcome the lithostatic component, the opening plane becomes horizontal, forming a sill (Vigneresse et al. 1999)

## 3.5 Dike Arrest

Eroded portions of extinct volcanic areas, as in eastern and western Iceland, show that most dikes become arrested in the crust and do not reach the surface to feed eruptions. Thus, some important mechanism determining dike arrest must exist. Since the possibility to have eruption is determined by the factors either encouraging dike propagation or determining dike arrest, understanding the conditions that lead to the stall of dikes may also allow better forecasting for eruptions.

Several factors may contribute in arresting a propagating dike. Among these is a poor or no contribution from any of the three factors affecting magmatic overpressure and thus dike propagation in Eq. 3.7: magmatic excess pressure, buoyancy and deviatoric stress. Decreasing magmatic excess pressure may be related to a reduced or chocked supply of magma from the source. The release of a limited amount of magma may induce the arrest of a dike or a magma-filled fracture at a finite distance from the source, consistently with observations at volcanoes (Taisne et al. 2011; Galetto et al. 2019). In fact, the smaller the volume of available magma, the more likely is that a dike stalls. There is indeed a minimum magma volume required for eruption as a function of magma buoyancy and source depth. The equation for this minimum volume $V_m$ of magma that allows eruption can be written as:

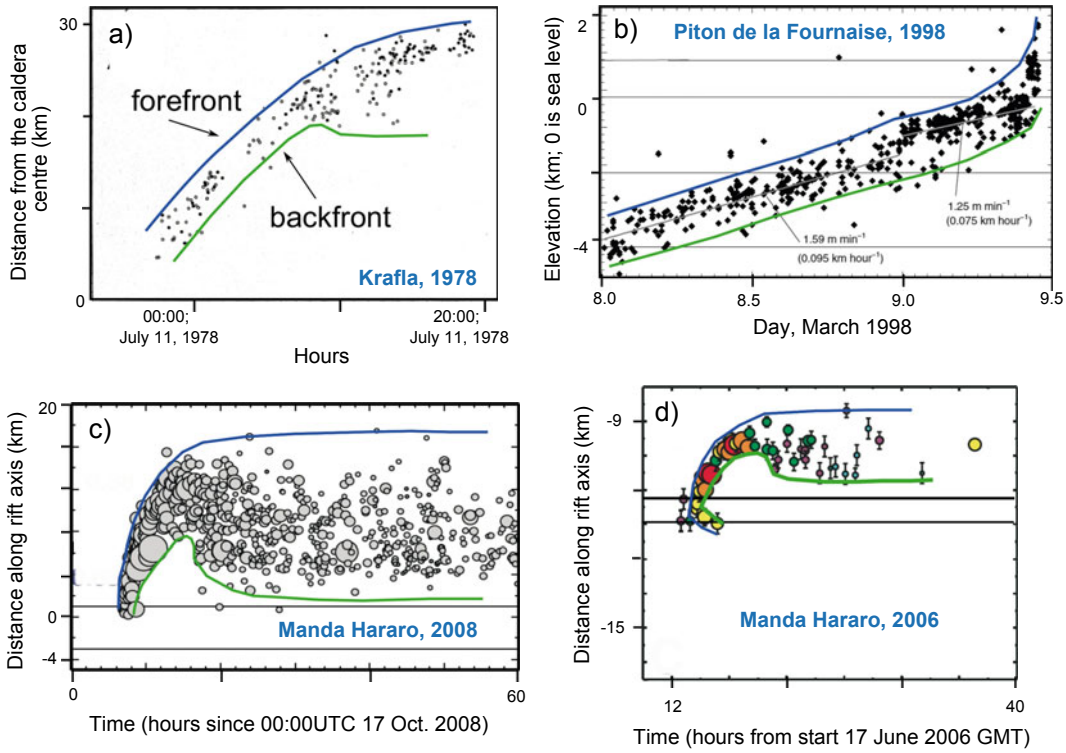


**Fig. 3.22** Seismicity patterns during different dike intrusions. **a** Seismicity induced by the 1978 lateral dike propagation at Krafla (Iceland); **b** seismicity induced by the 1998 vertical dike intrusion at Piton de la Fournaise (Reunion Island); **c** seismicity induced by dike 11 of the rifting episode in the Manda Hararo rift segment (Afar, Ethiopia); **d** seismicity induced by the 17 June 2006 dike of the rifting episode in the Manda Hararo rift segment (Afar, Ethiopia; Courtesy of Eleonora Rivalta; after Rivalta et al. 2015)

$$V_m = \left(\frac{z}{\zeta}\right)^4 \frac{(1-v)\Delta\rho g}{G} \qquad (3.15)$$

where $z$ *is* the source depth, $\zeta = 2L/b$ (where $2L$ is the dike length and $b$ is the dike width) and $G$ is the shear modulus of the country rock (Taisne et al. 2011). The resulting minimum magma volume that is required for eruption as a function of the depth of the magma source is shown in Fig. 3.23. In addition, any stratification of density will encourage the arrest of magma, so that, even with large volumes of magma available, eruption may be hindered by a shallow and thick low density layer, annulling magma buoyancy (Taisne et al. 2011). In this case, magma may accumulate in a swollen nose region at the base of the low density layer, where magma overpressure is largest and may become large

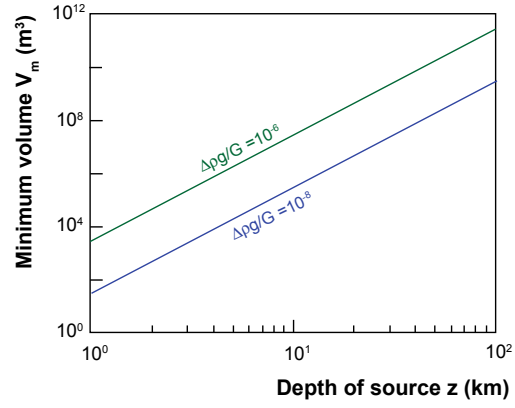


**Fig. 3.23** Diagram showing the minimum magma volume $V_m$ that is required for an eruption as a function of the depth of the magma source $z$. The two lines are drawn for two different values of $\Delta\rho g/G$ (where $\Delta\rho$ varies between 10 and 100 kg/m$^3$ and $G$ between $10^9$ and $10^{10}$ Pa; modified after Taisne et al. 2011)

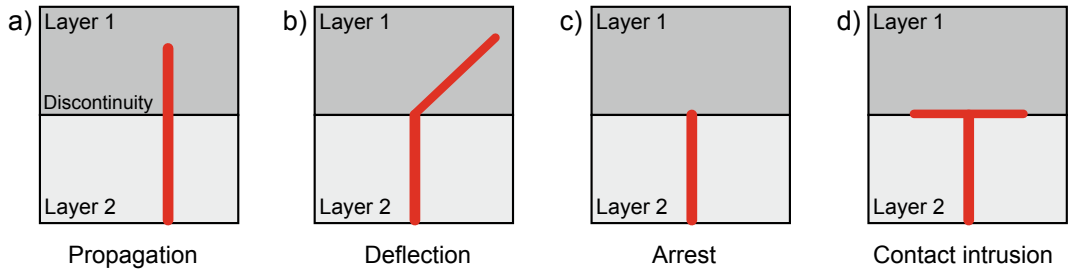


**Fig. 3.24** A dike (red line) meeting a discontinuity between two layers with different mechanical properties may propagate in the upper layer (**a**), be deflected in the upper layer (**b**), arrest at the contact (**c**) or intrude (symmetrically or not) along the contact, forming a sill (**d**)

enough to induce horizontal fractures in the dike walls and lateral propagation of a dike or a sill, preventing eruption. Also, magma ascent may be hindered by a compressive stress field in the upper crust, due to either large-scale tectonic forcing or loading by a tall volcanic edifice: this may decrease or nullify the deviatoric stress contribution in Eq. 3.7.

In addition to the factors included in Eq. 3.7, other conditions may promote the stalling of dikes. Among these are the cooling and solidification of the magma within the dike (which has been considered in Sect. 3.4.3) and the presence of pre-existing anisotropies (layering, fractures, faults) within the country rock. In particular, a significant amount of studies have been recently focusing on the role of subhorizontal crustal heterogeneities in controlling the propagation of dikes, promoting their deflection or arrest (Fig. 3.24). As for the deflection of dikes, mathematical simulations suggest that, when an inclined crack crosses a boundary between layers with different rigidity, a sudden change in the dip of the propagating crack occurs. If an inclined crack enters a softer medium, it becomes steeper, while if it enters a harder medium it becomes shallower. If the rigidity contrast is large, the crack may even become arrested forming a horizontal discontinuity along

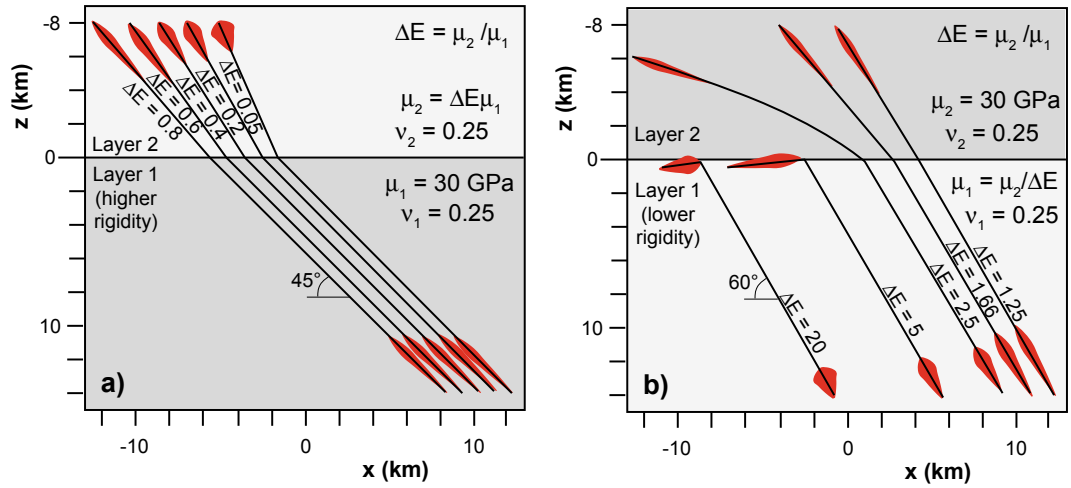


**Fig. 3.25** Modelling results showing the deflection of dikes (black lines) propagating through a layered medium with different rigidity contrasts given by $\Delta E = \mu_2/\mu_1$, where $\mu_2$ and $\mu_1$ are the rigidities of the upper and lower layers, respectively. **a** Deflection of dikes propagating at 45° passing from higher to lower rigidity medium; **b** Deflection of dikes propagating at 60° passing from lower to higher rigidity medium. The initial and final shapes of the dikes (in red) are exaggerated by a factor of 500 (modified after Maccaferri et al. 2010)

the interface (Fig. 3.25; Maccaferri et al. 2010). The arrest of dikes due to subhorizontal pre-existing structures can be achieved through two main conditions. A first is related to the presence of a mechanical layering within the country rock, also with layers sharing similar mechanical properties. In this case, any weak contact may open up as a result of dike-induced tensile stresses. This **Cook–Gordon mechanism** is likely to operate primarily at shallow depths, as supported by field observations and numerical models (Fig. 3.26a; Gudmundsson 2011). In particular, when a vertically propagating dike approaches a contact, especially in the uppermost 1–3 km of the crust, the dike-induced tensile stress may open up the contact before the dike-tip reaches it. In this mechanism the tensile strength of the contact determines if the debonding takes place. On meeting such an open contact, a dike may change into sill or become offset. This process may be more effective at a certain distance from the pressure source (as from a magma chamber), as the intensity of the tensile stress associated with a pressured magma chamber falls off rapidly with distance. A second condition for dike arrest due to pre-existing structures is related to the presence of a mechanical layering within the country rock with markedly different mechanical properties, as the stiffness of nearby layers (Gudmundsson 2002, 2006, 2011). Here **stress barriers** may develop along the contact between layers with relevant rigidity contrast, mainly through the rotation of the principal stresses. In fact, along a stress barrier the maximum principal stress $\sigma_1$ may become horizontal and the minimum principal stress $\sigma_3$ vertical (Fig. 3.26b). Since a dike is an extension fracture, it must propagate parallel to $\sigma_1$ and perpendicular to $\sigma_3$, thus potentially becoming a sill in correspondence with a stress barrier with vertical $\sigma_3$. In addition, abrupt changes in tensile stresses occur between layers of contrasting Young's moduli (**material-toughness** mechanism). These may develop both in passing from stiffer (higher Young's modulus) to softer (lower Young's modulus) layers and from softer to stiffer layers. However, a dike propagating through a softer layer

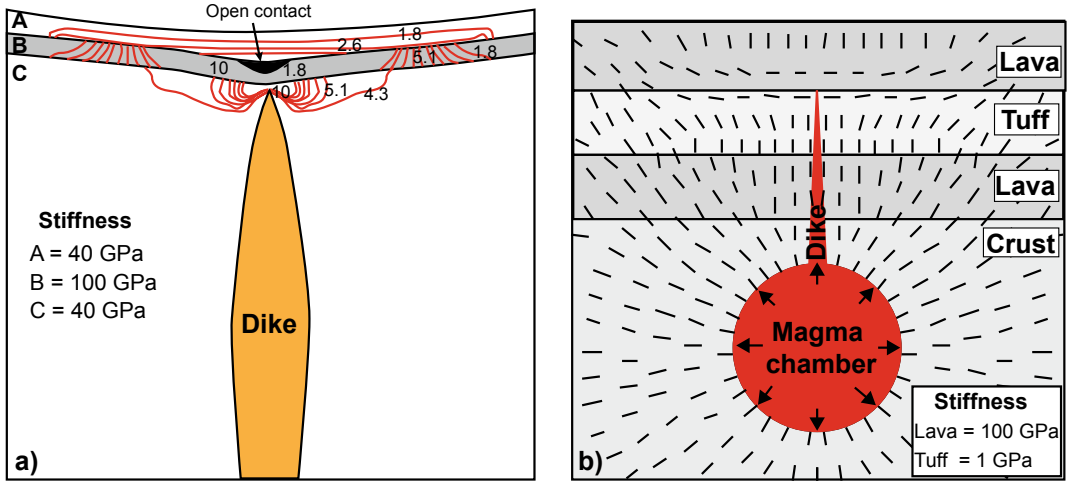


**Fig. 3.26** **a** Result of boundary-element model of the dike-induced tensile stresses (in MPa) and opening of a weak, shallow contact between mechanically dissimilar layers. Only a part of the stresses (in red) propagate through the upper layer, developing an open contact between layers. This model highlights the potential effects of the Cook–Gordon debonding mechanism for propagating dikes (modified after Gudmundsson 2011). **b** Finite-element model of the rotation of the maximum principal stress $\sigma_1$ (black lines) at the upper contact between a soft pyroclastic layer and a stiff lava flow. The only loading is the magmatic excess pressure in the chamber. This model suggests that, depending on the magmatic overpressure, the dike would either become deflected into the contact to form a sill or become arrested (modified after Gudmundsson 2011)

towards a stiffer layer would be more likely to deflect than a dike propagating from a stiffer layer towards a softer layer. Therefore, where softer layers, as for example clays or evaporites, underlie stiffer layers, as lava flows or intrusions, sheet and dike deflection or arrest are encouraged. Abrupt changes in stiffness between layers are also commonly associated with weak and partly open contacts and other discontinuities, especially at shallower crustal levels. In these conditions, a soft layer may not receive any significant tensile stress associated with the tip of a propagating dike, thus arresting it. Conversely, when the upper layer has similar stiffness to the lower layer (hosting the dike), there is little tendency for the dike to become deflected into the contact. These behaviours are supported by experiments on fracture propagation (Kavanagh et al. 2006; Menand 2008) and field evidence (Fig. 3.27; Klausen 2006; Gudmundsson 2011; Drymoni et al. 2020).

A further classical problem in dike propagation and arrest regards the role of high angle pre-existing structures, such as fractures and faults, in controlling the path of a dike. While most studies agree on the possibility that dikes penetrate pre-existing structures, the debate is largely on the real importance of this process for dike propagation (e.g., Ruch et al. 2016). A necessary condition for a dike to penetrate a pre-existing fracture (at the length scale of the dike) is that the magma pressure exceeds the ambient compression perpendicular to the fracture. If the magma pressure is only slightly greater than the least principal stress acting at the time of intrusion, then only fractures nearly perpendicular to the least principal stress can be dilated. If the magma

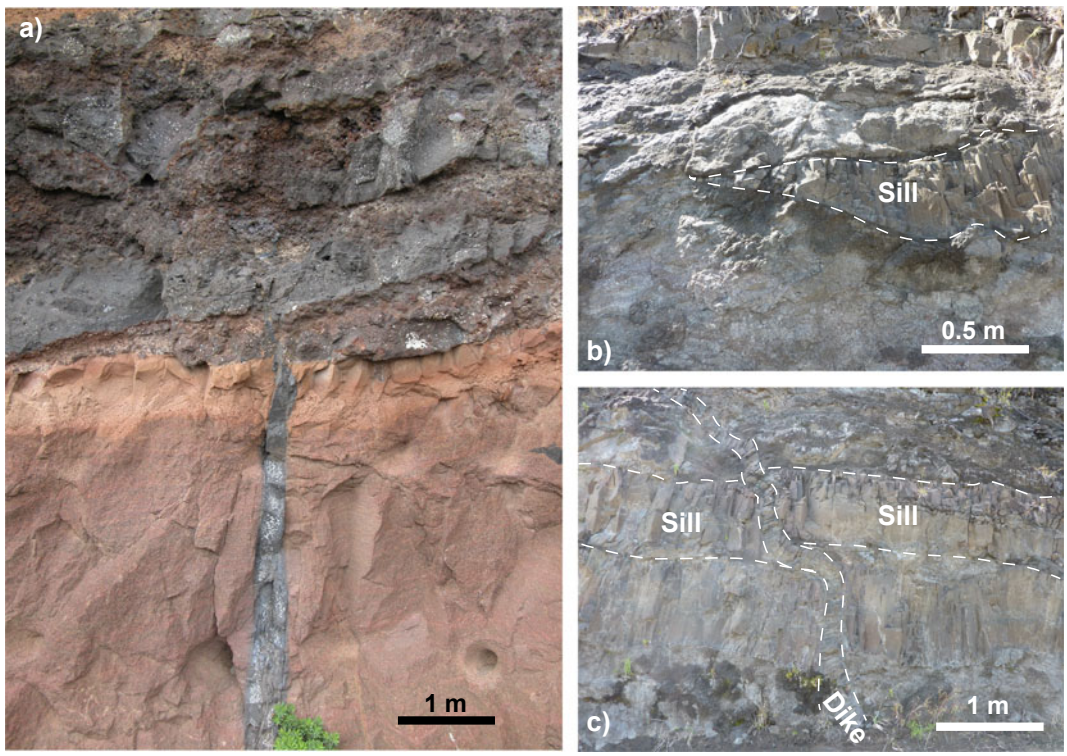


**Fig. 3.27** Field examples of terminations and captures of magma-filled fractures. **a** Dike arrested in correspondence of a change in lithology constituted by alternating lava flows and scoria layers, Tenerife (Canary Islands). **b** Lateral sharp termination of a sill, Piton des Neiges (La Reunion Island). **c** Dike partially deflected horizontally in correspondence of the lower margin of a sill, Piton des Neiges (La Reunion Island). Approximate scales are given

pressure exceeds the maximum principal stress, then fractures of any orientation can be dilated (Delaney et aI. 1986; Rubin 1995b). However, in this case a dike may not penetrate such a fracture for long. If the fracture is not aligned with the principal stresses and the ratio of shear to opening of the dike walls is not small, the shear stress concentration at the tip fractures intact rock, determining the new direction of propagation. In addition, for a dike to intrude a pre-existing fracture, the effective ambient dike-normal stress should be small compared to the tensile strength of the country rock. This condition is not easily met at mid- to lower-crustal levels, where the

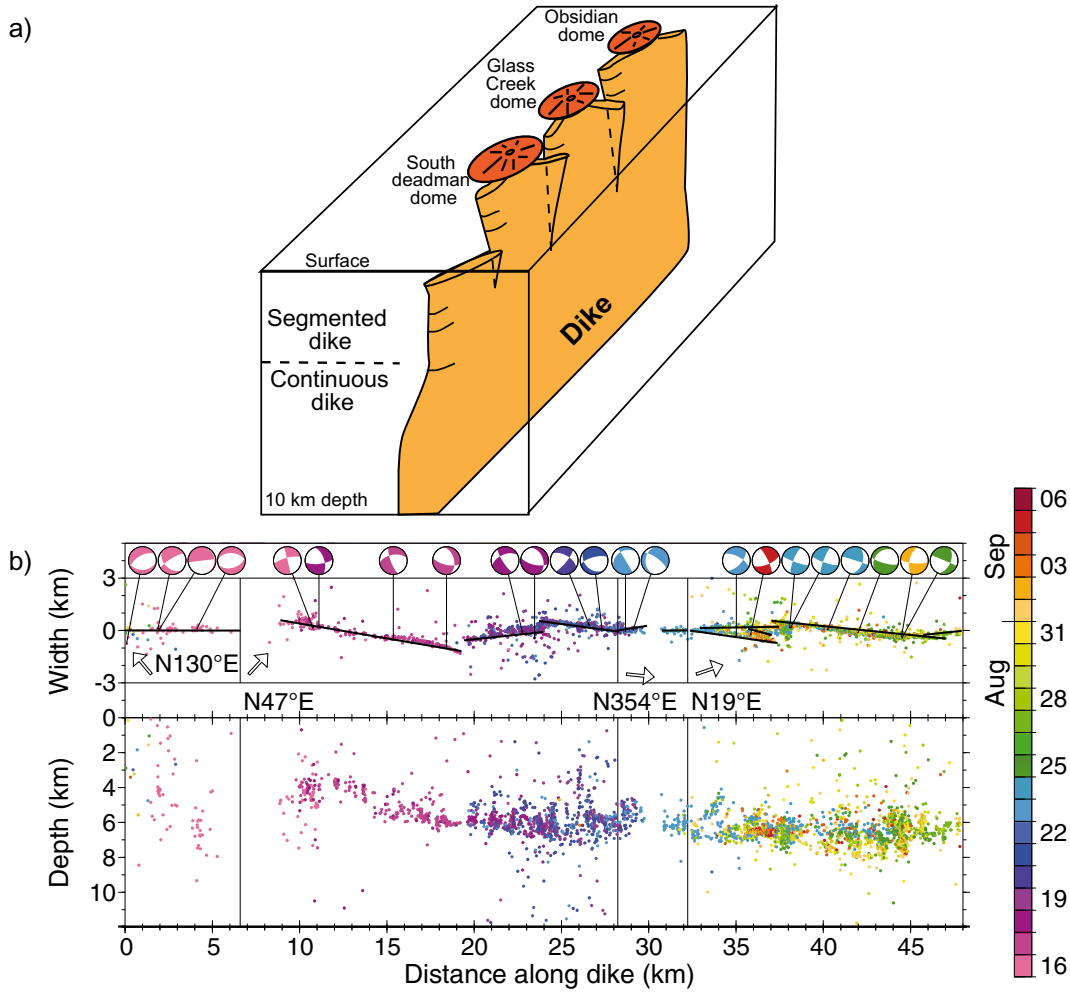


**Fig. 3.28** **a** Three-dimensional view of the reconstructed segmented Inyo dike nearby Long Valley caldera (California; USA; modified after Reches and Fink 1988). **b** Seismicity along the Bardarbunga (Iceland) dike, 16 August–6 September 2014. Top: Plan-view of four rotated areas along the dike; arrows indicate geographic north. Coloured dots (for timing see reference bar to the right) denote epicentres and black lines dike segments; focal mechanisms for selected earthquakes are also shown. Bottom: earthquake depths referenced to sea level (modified after Sigmundsson et al. 2015. Image courtesy: Freysteinn Sigmundsson)

high ambient dike normal stress becomes significant, unless there is an abnormally high pore pressure. Studies studies also highlight the importance of the dip of a fault in the fault being captured by a dike, a process mainly occurring for steeply-dipping faults (Ziv et al. 2000; Gaffney et al. 2007). According to other studies, since the fracture strength of the country rock provides negligible resistance to dike propagation, there is little mechanical advantage in intruding along pre-existing fractures. As a consequence, the orientation of a dike will mainly depend upon the direction of the regional stresses (Lister and Kerr 1991). The relative independence of dike propagation from pre-existing fractures is also consistent with the evidence that, in faulted rift zones, most monogenic cones tend to cluster at a small distance (few hundred of m) from a fault, on its foot wall, and not along the fault (Maccaferri et al. 2015). In some cases the presence of faults may even hinder or arrest dike propagation. This has been proposed for Miyakejima (Japan) in 2000, when a pre-existing strike-slip fault, pre-loaded with significant stress, released gradually its energy during the interplay with a dike propagating laterally and perpendicularly to it, confining dike propagation. Quite similarly, the slip along the graben faults developed above a vertically propagating dike in 2009 at Harrat Lunayyir (Saudi Arabia) induced compression above the upper tip of the dike, holding back its further propagation (Maccaferri et al. 2016; Xu et al. 2016). In other cases, the interaction between a dike and nearby parallel pre-existing fractures may induce a change in the trajectory or the decrease in velocity and propagation of the dike, as suggested by analogue models (Le Corvec et al. 2013).

Finally, many dikes are often segmented in section (Fig. 3.9b) or, more commonly, in map view, especially at shallow crustal levels, with the segmentation highlighted by the distribution of seismicity and/or the distribution and orientation of vents forming fissure eruptions. Segmentation commonly develops dikes with en-echelon configuration, where each dike segment is offset, also with slightly different orientation, with regard to the previous one. This is interpreted to result from the rotation of the stresses or, equivalently, from a mixed mode of fracture, including opening (Mode I) and tearing (Mode III) of the dike tip. The angle of the segments relative to the overall strike of the array of en-echelon dikes is related to the rotation angle of the stress and to the extensional to shear stress ratio (Pollard et al. 1982; Rivalta et al. 2015). Segmentation is commonly observed at the tip of extension fractures, as for example when forming plumose structures. Similarly to extension fractures, each segment of a dike may be considered as branching from a single common parent structure at depth, as postulated for the Inyo dike nearby Long Valley caldera (California, USA; Fig. 3.28a; Reches and Fink 1988). Segmentation has been also observed along the nearly 50 km long Bardarbunga (Iceland) dike developed in 2014. In this case, the distribution of the seismicity allowed highlighting at least 6 major offset segments, each with different orientation (Fig. 3.28b; Sigmundsson et al. 2015).

## 3.6 Summary

This chapter has shown how magma may rise in the crust through different mechanisms, mainly depending upon its composition, temperature, crystallization and strain rate, and the physical (mechanical and thermal) state of the crust. In a lower crust experiencing ordinary thermal conditions, diking and diapirism are both viable processes for the rise of magma. As for the role of magma composition, while the less viscous mafic dikes have little difficulty leaving the source region, the more viscous felsic dikes freeze soon after the magma encounters rock at temperatures below the magma solidus. As a result, the rise through larger diapirs, cooling less rapidly, is more common in felsic magma. Magma temperature has a similar effect, with hotter magma expected to rise through dikes and relatively colder magma rising mainly through diapirs. Also, magma too crystalline (>25%) may not continue the ascent through dikes, but only through diapirs. However, with significant crystallization (>70%) diapiric ascent is prevented and any further magma injection may inflate the

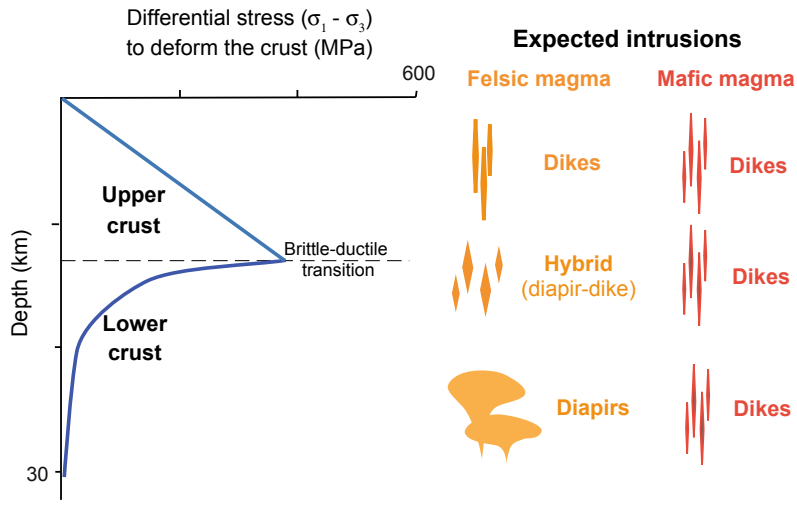


**Fig. 3.29** Summary of the expected dominant intrusions accompanying the rise of magma in the upper brittle crust (dikes), in the lower viscous crust (dikes and diapirs) and along the brittle-ductile transition (hybrid and dikes)

diapir through ballooning (Bateman 1985). High strain rates induced by magmatic overpressures (in the range of $10^{-10}$ to $10^{-12}$ $s^{-1}$) promote elastic-brittle deformation, thus enhancing diking (DeSaint Blanquat et al. 2001).

These conditions imply that in the lower crust dikes are commonly associated with the less viscous mafic magmas, whereas diapirs are usually associated with the more viscous felsic magmas. However, hybrid mechanisms of ascent involving thicker dikes (aspect ratio on the order of $10^{-1}$ to $10^{-2}$) may be also found, especially approaching the brittle-ductile transition (Fig. 3.29). In fact, at the brittle-ductile transition there is a rapid increase in the strength of the crustal rocks, so that in the upper brittle crust the ascent of buoyant diapirs is inhibited and the further rise of magma occurs through dikes, independently of the composition. Felsic and/or colder dikes must be thicker to survive freezing and usually propagate to shorter distances. Mafic and/or hotter magmas can propagate through thinner dikes to farther distances. Magma transfer through dike propagation, being widespread in the brittle upper crust, is thus of particular interest for volcano-tectonic processes, especially those leading to eruption. Dike propagation can be conveniently described considering both a solid and a fluid mechanics approach. The former focuses on the elastic behaviour of the country rock and the non-elastic behaviour at the dike tip, where the stress intensity factor competes with the fracture toughness of the country rock. The fluid mechanics approach considers the competition between the factors that allow the propagation of magma (summarised in the concept of magma overpressure) and the resisting factors (as the viscous pressure drop of the magma). For a complete analysis, the thermal interactions between the magma and the country rock, as deriving from conduction of heat, should be also considered. In addition to the factors controlling dike propagation, those controlling dike arrest should be also taken into account: these may be related to an insufficient magmatic overpressure and/or to the presence of mechanical anisotropies in the country rock. Indeed, it is the knowledge of the conditions determining both the propagation and arrest of dikes that allows understanding shallow magma transfer and ultimately help in forecasting eruptions.

## 3.7 Main Symbols Used

| | |
|---|---|
| $b$ | Dike width or breadth |
| $C_p$ | Heat capacity |
| $d_s$ | Thickness of softened region |
| $E_s$ | Elastic stiffness of the host rock |
| $g$ | Acceleration due to gravity |
| $G$ | Rigidity or shear modulus of the host rock |

| | |
|---|---|
| $h$ | Dike height |
| $K$ | Stress intensity factor |
| $K_c$ | Fracture toughness |
| $L$ | Half-length of the dike |
| $L_p$ | Propagation distance |
| $P$ | Magma pressure |
| $P_e$ | Excess magma pressure |
| $P_s$ | Tip suction |
| $P_t$ | Pressure at tip cavity |
| $Q_f$ | Volumetric flow rate |
| $r$ | Diapir radius |
| $t$ | Time |
| $T_u$ | Thickness of upper layer |
| $U_a$ | Ascent velocity |
| $U_d$ | Velocity of magma within the dike |
| $V_m$ | Minimum volume of magma that allows eruption |
| $w$ | Half-thickness of dike |
| $w_f$ | Thickness of frozen margin of dike |
| $z$ | Source depth |
| $Z_v$ | Parameter describing the increase in viscosity |
| $\alpha$ | Thermal diffusivity |
| $\Delta P/2L$ | Pressure gradient |
| $\Delta P_d$ | Viscous pressure drop |
| $\Delta P_m$ | Magmatic overpressure |
| $\Delta\rho$ | Density contrast between magma and host rock |
| $\Delta\sigma$ | Difference between far-field vertical and horizontal principal stresses |
| $\zeta$ | Dimensionless parameter |
| $\eta$ | Viscosity |
| $\lambda$ | Numerical coefficient |
| $v$ | Poisson's ratio |
| $\Pi$ | Dimensionless parameter |
| $\rho_1$ | Density of the upper layer |
| $\rho_2$ | Density of the lower layer |
| $\rho_m$ | Intrusion density |
| $\rho_r$ | Country rock density |
| $\sigma_1$ | Maximum principal stress |
| $\sigma_2$ | Intermediate principal stress |
| $\sigma_3$ | Minimum principal stress |
| $\sigma_h$ | Far-field horizontal principal stress |
| $\sigma_n$ | Ambient compressive stress perpendicular to the dike |
| $\sigma_v$ | Far-field vertical principal stress |

## References


Ágústsdóttir T, Woods J, Greenfield T, Green RG, White RS, Winder T et al (2016) Strike-slip faulting during the 2014 Bardarbunga-Holuhraun dike intrusion, central Iceland. Geophys Res Lett 43:1495–1503

Ahmed A, Doubre C, Leroy S, Kassim M, Keir D, Abayazid A et al (2016) Seafloor spreading event in western Gulf of Aden during the November 2010–March 2011 period captured by regional seismic networks: evidence for diking events and interactions with a nascent transform zone. Geophys J Int 205:1244–1266

Bateman R (1984) On the role of diapirism in the segregation, ascent and final emplacement of granitoid magmas. Tectonophysics 110:211–231

Bateman R (1985) Progressive crystallization of a granitoid diapir and its relationship to stages of emplacement. J Geol 93:645–662

Belachew M, Ebinger C, Cote D (2013) Source mechanisms of dike-induced earthquakes in the Dabbahu-Manda Hararo rift segment in Afar, Ethiopia: implications for faulting above dikes. Geophys J Int 192:907–917

Berner H, Ramberg H, Stephansson O (1972) Diapirism in theory and experiment. Tectonophysics 15:197–218

Biot MA, Odè H (1965) Theory of gravity instability with variable overburden and compaction. Geophysics 30:213–227

Bittner D, Schmeling H (1995) Numerical modelling of melting processes and induced diapirism in the lower crust. Geophys J Int 123:59–70

Bonaccorso A, Aoki Y, Rivalta E (2017) Dike propagation energy balance from deformation modelling and seismic release. Geophys Res Lett 44:5486–5494

Bruce PM, Huppert HE (1989) Thermal control of basaltic fissure eruptions. Nature 342:665–667

Burov E, Jaupart C, Guillou-Frottier L (2003) Ascent and emplacement of buoyant magma bodies in brittle-ductile upper crust. J Geophys Res 108:2177. https://doi.org/10.1029/2002JB001904

Cao W, Kaus BJP, Paterson S (2016) Intrusion of granitic magma into the continental crust facilitated by magma pulsing and dike-diapir interactions: numerical simulations. Tectonics 35:1575–1594

Carslaw HS, Jaeger JC (1959) Conduction: heat in solids. Oxford Clarendon, 2nd edn, 510 pp

Chen Z, Jin ZH, Johnson SE (2011) Transient dike propagation and arrest near the level of neutral buoyancy. J Volcanol Geoth Res 203:81–86

Cruden AR (1988) Deformation around a rising diapir modeled by creeping flow past a sphere. Tectonics 7:1091–1101

Daniels KA, Kavanagh JL, Menand T, Sparks RSJ (2012) The shapes of dikes: evidence for the influence of cooling and inelastic deformation. Geol Soc Am Bull 124:1102–1112

Delaney PT, Pollard DD (1982) Solidification of basaltic magma during flow in a dike. Am Journ Science 282:856:885

Delaney PT, Pollard DD, Ziony JI, McKee EH (1986) Field relations between dikes and joints' emplacement processes and paleostress analysis. J Geophys Res 91:4920–4938

de Saint Blanquat M, Law RD, Bouchez JL, Morgan SS (2001) Internal structure and emplacement of the Papoose Flat pluton: an integrated structural, petrographic and magnetic susceptibility study. Geol Soc Am Bull 113:976–995

Dixon JM (1975) Finite strain and progressive deformation in models of diapiric structures. Tectonophysics 28:89–124

Drymoni K, Browning J, Gudmundsson A (2020) Dyke-arrest scenarios in extensional regimes: insights from field observations and numerical models, Santorini, Greece. J Volcanol Geoth Res 396:106854

Dumond G, Yoshinobu AS, Barnes CG (2005) Midcrustal emplacement of the Sausfjellet pluton, central Norway: ductile flow, stoping, and in situ assimilation. Geol Soc Am Bull 117:383–395

Emerman SH, Marrett R (1990) Why dikes? Geology 18:231–233

England RW (1990) The identification of granitic diapirs. J Geol Soc London 147:931–933

England RW (1992) The genesis, ascent and emplacement of the Northern Arran Granite, Scotland: implications for granitic diapirism. Geol Soc Am Bull 104:606–614

Eyles JHW, Illsley-Kemp F, Keir D, Ruch J, Jónsson S (2018) Seismicity associated with the formation of a New Island in the Southern Red Sea. Front Earth Sci 6:141. https://doi.org/10.3389/feart.2018.00141

Fialko Y, Pearse J (2012) Sombrero uplift above the Altiplano-Puna magma body: evidence of a ballooning mid-crustal diapir. Science 338:250–252

Gaffney EF, Damjanac B, Valentine GA (2007) Localization of volcanic activity: 2. Effects of pre-existing structure. Earth Planet Sci Lett 263:323–338

Galadi Enriquez E, Galindo Zaldivar J, Simancas F, Exposito I (2003) Diapiric emplacement in the upper crust of a granitic body: the La Bazana granite (SW Spain). Tectonophysics 361:83–96

Galetto F, Bagnardi M, Acocella V, Hooper A (2019) Noneruptive unrest at the caldera of Alcedo Volcano (Galápagos Islands) revealed by InSAR data and geodetic modeling. J Geophys Res 124. https://doi.org/10.1029/2018JB017103

Glazner AF, Miller DM (1997) Late-stage sinking of plutons. Geology 25:1099–1102

Glazner AF, Bartley JM (2006) Is stoping a volumetrically significant pluton emplacement process? Geol Soc Am Bull 118:1185–1195

Glazner AF, Bartley JM (2008) Reply to comments on "is stoping a volumetrically significant pluton emplacement process?" Geol Soc Am Bull 120:1082–1087

Gonnermann H, Taisne B (2015) Magma transport in dikes. In: Sigurdsson H, Houghton B, McNutt S, Rymer H, Stix J (eds) The encyclopedia of volcanoes, 2nd edn. Elsevier Academic Press, pp 215–224

Grandin R, Jacques E, Nercessian A, Ayele A, Doubre C, Socquet A et al (2011) Seismicity during lateral dike propagation: insights from new data in the recent Manda Hararo–Dabbahu rifting episode (Afar, Ethiopia). Geochem Geophys Geosyst 12: Q0AB08. https://doi.org/10.1029/2010GC003434

Gressier JB, Mourgues R, Bodet L, Matthieu JY, Galland O, Cobbold P (2010) Control of pore fluid pressure on depth of emplacement of magmatic sills: an experimental approach. Tectonophysics 489:1–13

Gudmundsson A (1990) Emplacement of dikes, sills and crustal magma chambers at divergent plate boundaries. Tectonophysics 176:257–275

Gudmundsson A, Marinoni LB, Marti J (1999) Injection and arrest of dykes: implications for volcanic hazards. J Volcanol Geoth Res 88:1–13

Gudmundsson A (2002) Emplacement and arrest of sheets and dykes in central volcanoes. J Volcanol Geoth Res 116:279–298

Gudmundsson A (2006) How local stresses control magma-chamber ruptures, dyke injections, and eruptions in composite volcanoes. Earth Sci Rev 79:1–31

Gudmundsson A (2011) Rock fractures in geological processes. Cambridge University Press 569 pp

Hawkins DP, Wiebe RA (2004) Discrete stoping events in granite plutons: a signature of eruptions from silicic magma chambers? Geology 32:1021–1024

He B, Xu Y, Paterson S (2009) Magmatic diapirism of the Fangshan pluton, southwest of Beijing, China. J Struct Geol 31:615–626

Henderson ST, Pritchard ME (2013) Decadal volcanic deformation in the Central Andes Volcanic Zone revealed by InSAR time series. Geochem Geophys Geosyst 14:1358–1374

Jackson MPA, Talbot CJ (1986) External shapes, strain rates, and dynamics of salt structures. Geol Soc Am Bull 97:305–323

Jaeger JC (1969) Elasticity, Fracture and Flow, with engineering and geological applications. Springer Netherlands 268 pp, https://doi.org/10.1007/978-94-011-6024-7

Jellinek AM, De Paolo DJ (2003) A model for the origin of large silicic magma chambers: precursors of caldera-forming eruptions. Bull Volcanol 65:363–381

Kavanagh JL, Menand T, Sparks RSJ (2006) An experimental investigation of sill formation and propagation in layered elastic media. Earth Planet Sci Lett 245:799–813

Kjoll HJ, Galland O, Labrousse L, Andersen TB (2019) Emplacement mechanisms of a dyke swarm across the brittle-ductile transition and the geodynamic implications for magma-rich margins. Earth Planet Sci Lett 518:223–235

Klausen MB (2006) Geometry and mode of emplacement of dike swarms around the Birnudalstindur igneous centre, SE Iceland. J Volcanol Geoth Res 151:340–356

Krumbholz M, Hieronymous CF, Burchardt S, Troll VR, Tanner DC, Friese N (2014) Weibull-distributed dyke thickness reflects probabilistic character of host-rock strength. Nat Commun 5:3272. https://doi.org/10.1038/ncomms4272

Le Corvec N, Menand T, Lindsay J (2013) Interaction of ascending magma with pre-existing crustal fractures in monogenetic basaltic volcanism: an experimental approach. J Geophys Res 118:968–984

Lister JR, Kerr RC (1991) Fluid-mechanical models of crack propagation and their application to magma transport in dikes. J Geophys Res 96:10049–10077

Lister JR (1995) Fluid-mechanical models of the interaction between solidification and flow in dykes. In: Baer, Heimann (eds) Physics and chemistry of dykes. Balkema Rotterdam, pp 115–124. ISBN 9054105518

Maccaferri F, Bonafede M, Rivalta E (2010) A numerical model of dyke propagation in layered elastic media. Geophys J Int 180:1107–1123

Maccaferri F, Acocella V, Rivalta E (2015) How the differential load induced by normal fault scarps controls the distribution of monogenic volcanism. Geophys Res Lett 42. https://doi.org/10.1002/2015GL065638

Maccaferri F, Rivalta E, Passarelli L, Aoki Y (2016) On the mechanisms governing dike arrest: insight from the 2000 Miyakejima dike injection. Earth Planet Sci Lett 434:64–74

Mahon KI, Harrison TM, Drew DA (1988) Ascent of a granitoid diapir in a temperature varying medium. J Geophys Res 93:1174–1188

Marsh BD (1982) On the mechanics of igneous diapirism, stoping, and zone melting. Am J Sci 282:808–855

Menand T (2008) The mechanics and dynamics of sills in elastic layered media and their implications for the growth of laccoliths. Earth Planet Sci Lett 267:93–99

Miller RB, Paterson SR (1999) In defense of magmatic diapirs. J Struct Geol 21:1161–1173

Molyneux SJ, Hutton DHW (2000) Evidence for significant granite space creation by the ballooning mechanism: The example of the Ardara pluton, Ireland. Geol Soc Am Bull 112:1543–1558

Passarelli L, Rivalta E, Cesca S, Aoki Y (2015) Stress changes, focal mechanisms, and earthquake scaling laws for the 2000 dike at Miyakejima (Japan). J Geophys Res 120:4130–4145

Paterson SR, Vernon RH (1995) Bursting the bubble of ballooning plutons: a return to nested diapirs emplaced by multiple processes. Geol Soc Am Bull 107:1356–1380

Paterson SR, Fowler TK (1996) Local displacement of diapir contacts and its importance to pluton emplacement study: discussion. J Struct Geol 18:711–712

Paterson SR, Miller RB (1998a) Stoped blocks in plutons: paleo-plumb bobs, viscometers, or chronometers? J Struct Geol 20:1261–1272

Paterson SR, Miller RB (1998b) Mid-crustal magmatic sheets in the Cascades Mountains, Washington: implications for magma ascent. J Struct Geol 20:1345–1363

Paterson SR, Farris DW (2006) Downward host rock transport and the formation of rim monoclines during the emplacement of Cordilleran batholiths. Trans Roy Soc Edinburgh Earth Sci 97:397–413

Paterson SR, Pignotta GS, Farris D, Memeti V, Miller RB, Vernon RH et al (2008) Is stoping a volumetrically significant pluton emplacement process? Discussion. Geol Soc Am Bull 120:1075–1079

Pollard DD, Segall P, Delaney PT (1982) Formation and interpretation of dilatant echelon cracks. Geol Soc Am Bull 93:1291–1303

Ramberg H (1981) Gravity, deformation and the Earth's crust in theory, experiments and geological applications. Academic Press, London

Ramsay JG (1989) Emplacement kinematics of a granite diapir: the Chindamora batholith, Zimbabwe. J Struct Geol 11:191–209

Reches Z, Fink J (1988) The mechanism of intrusion of the Inyo Dike, Long Valley Caldera, California. J Geophys Res 93:4321–4334

Rivalta E, Taisne B, Bunger AP, Katz RF (2015) A review of mechanical models of dike propagation: schools of thought, results and future directions. Tectonophysics 638:1–42

Roman DC, Moran SC, Power JA, Cashman KV (2004) Temporal and spatial variation of local stress fields before and after the 1992 Eruptions of Crater Peak Vent, Mount Spurr Volcano, Alaska. Bull Seismol Soc Am 94:2366–2379

Rosenberg CL, Berger A, Schmid SM (1995) Observations from the floor of a granitoid pluton: inferences on the driving force of final emplacement. Geology 23:443–446

Rubin AM, Gillard D (1988) Dike-induced earthquakes: theoretical considerations. J Geophys Res 103:10017–10030

Rubin AM (1993) Dikes versus diapirs in viscoelastic rock. Earth Planet Sci Lett 119:641–659

Rubin AM (1995a) Getting granite dikes out of the source region. J Geophys Res 100:5911–5929

Rubin AM (1995b) Propagation of magma-filled cracks. Annual Rev Earth Planet Sci 23:287–336

Ruch J, Wang T, Xu W, Hensch M, Jonsson S (2016) Oblique rift opening revealed by reoccurring magma injection in central Iceland. Nat Commun 7:12352. https://doi.org/10.1038/ncomms12352

Sakuma S, Kajiwara T, Nakada S, Uto K, Shimizu H (2008) Drilling and logging results of USDP-4—penetration into the volcanic conduit of Unzen Volcano, Japan. J Volcanol Geoth Res 175:1–12

Segall P, Llenos AL, Yun S-H, Bradley AM, Syracuse EM (2013) Time-dependent dike propagation from joint inversion of seismicity and deformation data. J Geophys Res 118:5785–5804

Sigmundsson F, Hooper A, Hreinsdóttir S, Vogfjörd KS, Ófeigsson BG, Heimisson ER et al (2015) Segmented lateral dyke growth in a rifting event at Bardarbunga volcanic system, Iceland. Nature 517:191–195

Sumita I, Ota Y (2011) Experiments on buoyancy-driven crack around the brittle–ductile transition. Earth Planet Sci Lett 304:337–355

Taisne B, Jaupart C (2009) Dike propagation through layered rocks. J Geophys Res 114:B09203

Taisne B, Tait S, Jaupart C (2011) Conditions for the arrest of a vertical propagating dyke. Bull Volcanol 73:191–204

Turcotte DL, Schubert G (1982) Geodynamics: application of continuum physics to geological problems. John Wiley, NY, 450 pp

Urbani S, Acocella V, Rivalta E (2018) What drives the lateral versus vertical propagation of dikes? Insights from analogue models. J Geophys Res 123. https://doi.org/10.1029/2017JB015376

Vigneresse JL (1995) Crustal regime of deformation and ascent of granitic magma. Tectonophysics 249:187–202

Vigneresse JL, Tikoff B, Améglio L (1999) Modification of the regional stress field by magma intrusion and formation of tabular granitic plutons. Tectonophysics 302:203–224

Wada Y (1994) On the relationship between dike width and magma viscosity. J Geophys Res 99:17743–17755

Weinberg RF, Podladchikov Y (1994) Diapiric ascent of magmas through power law crust and mantle. J Geophys Res 99:9543–9559

Woods J, Winder T, White RS, Bransdottir B (2019) Evolution of a lateral dike intrusion revealed by relatively-relocated dike-induced earthquakes: the 2014–15 Bárdarbunga-Holuhraun rifting event, Iceland. Earth Planet Sci Lett 506:53–63

Yoshinobu AS, Barnes CG (2008) Is stoping a volumetrically significant pluton emplacement process? Discussion. Geol Soc Am Bull 120:1080–1081

Xu W, Jónsson S (2014) The 2007–8 volcanic eruption on Jebel at Tair island (Red Sea) observed by satellite radar and optical images. Bull Volcanol 76:795

Xu W, Jónsson S, Ruch J, Aoki Y (2016) The 2015 Wolf volcano (Galápagos) eruption studied using Sentinel-1 and ALOS-2 data. Geophys Res Lett 43:9573–9580

Zak J, Paterson SR (2006) Roof and walls of the Red Mountain Creek pluton, eastern Sierra Nevada, California (USA): implications for process zones during pluton emplacement. J Struct Geol 28:575–587

Zak J, Vemer K, Johnson K, Schwartz JJ (2012) Magma emplacement process zone preserved in the roof of a large Cordilleran batholith, Wallowa Mountains, northeastern Oregon. J Volcanol Geoth Res 227–228:61–75

Ziv A, Rubin AM, Agnon A (2000) Stability of dike intrusion along preexisting fractures. J Geophys Res 105:5947–5961